CZECH TECHNICAL UNIVERSITY IN PRAGUE
Faculty of Nuclear Sciences and Physical Engineering
Department of Physical Electronics

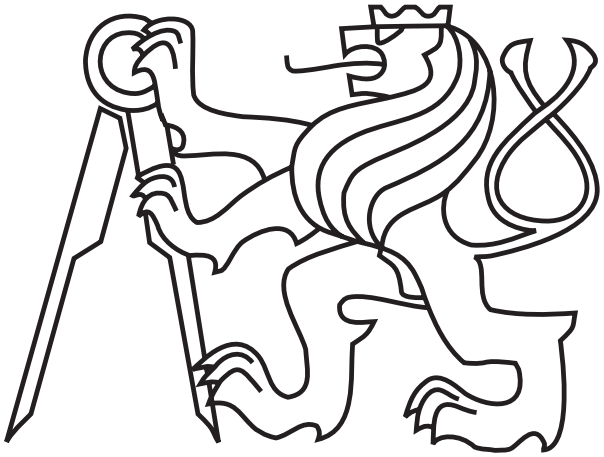

STUDY TO DOCTORAL THESIS

High Energy X-Ray Sources from Laser Plasmas

Author: Ing. Vojtěch Horný
Supervisor: Doc. Ing. Ondřej Klimo, Ph.D.
Supervisor specialist: Ing. Jaroslav Nejdl, Ph.D.

June 30, 2016

Title: **High Energy X-Ray Sources from Laser Plasmas**

Author: **Ing. Vojtěch Horný**
Department of Physical Electronics
Faculty of Nuclear Sciences and Physical Engineering
Czech Technical University in Prague
Trojanova 13, 120 00 Praha 2, Czech Republic

Supervisor: **doc. Ing. Ondřej Klimo, Ph.D.**
Department of Physical Electronics
Faculty of Nuclear Sciences and Physical Engineering
Czech Technical University in Prague
Trojanova 13, 120 00 Praha 2, Czech Republic

Supervisor specialist: **Ing. Jaroslav Nejdl, Ph.D.**
Institute of Physics CAS, v. v. i./ ELI Beamlines
Za Radnicí 835, 252 41 Dolní Břežany, Czech Republic

Abstract: The considered sources of high energy X-rays from laser plasmas are discussed in this study to doctoral thesis. Since they are mostly based on the acceleration of electrons after laser plasma interaction, a lot of attention is paid to the laser wakefield acceleration mechanism. The method to improve the properties of produced electron bunches using crossed laser beams is suggested and compared with other considered optical injection configurations. The influence on generated x-rays is accented. The theory of radiation emitted by moving charge is reviewed and the code calculating radiation features is proposed, implemented, tested, and applied. The new method to construct the spectrograms of betatron radiation in the wiggler regime is introduced. Although the work is based mainly on numerical simulations, the contact with the experiment is still maintained. The simulations relevant to the experimental campaign run at Ti:sapphire laser system located at the PALS laboratory are included.

Contents

Chapter 1

Introduction

X-Ray radiation is generally defined as the part of electromagnetic spectrum with energies higher than 250 eV, or equivalently with the corresponding wavelength lower than 5 nm. This broad region can be divided into two parts, soft X-rays with the energy up to several keV, and more energetic hard X-rays [Attwood, 2007]. In this thesis we will mostly operate on this very uncertain border.

X-ray radiation since its discovery by Wilhelm Conrad Röntgen in 1895 is being used as a mighty tool to investigate the properties of matter. It is being extensively used in various branches, including with the fundamental scientific research, the medical and industrial applications and the public security.

Nowadays, X-ray radiation is delivered by radioactive sources, X-ray tubes and devices based on classical electron accelerators such as synchrotron. There are various ways how to generate X-rays from accelerated electron bunch. The simplest one is to use the incurvation of the electron trajectory in the synchrotron to generate so called synchrotron radiation. Rather more sophisticated mechanism is to use the periodical magnetic structures to force the accelerated electrons to undergo the transverse oscillations during their straight propagation and to radiate the X-rays thereby. These devices are called undulators or wigglers, the main difference between them is in the amplitude of deviation from the straight line path of the electrons.

Nevertheless, despite great progress in the technology there is still demand for the upgrades of X-ray sources. Firstly, the shortening of the X-ray pulses durations to the order of units or at least tens of femtoseconds is a great challenge which could offer novel applications. Nowadays, the shortest pulse durations achievable by standard synchrotron facilities are subpicosecond [Schick et al., 2016, Schoenlein et al., 2000, Khan et al., 2006], this rather intricate technique is called sliced synchrotron beamlines. For instance, the duration of typical vibrational period in the atoms is in the order of tens of femtoseconds as well. Once having an X-ray source producing even shorter pulses, the fundamental physical processes such as electron transfer, lattice vibrations, phase transitions, chemical

reactions and a spin dynamics could be sampled and therefore possibly better understood. This would possibly result in further progress in another disciplines and bring new applications.

Secondly, reducing of the size of the X-ray source is another meaningful goal. Micron source size would lead to the enhancement of the resolution of the sampled images in comparison with absorption radiography using conventional X-ray tubes.

All considered sources of X-rays from laser plasma are based on the generation of the accelerated electron bunches from the laser plasma interaction. Currently, the most promising way is laser wakefield acceleration mechanism. This concept is introduced in the chapter 2 together with the discussion of the limitation of the 20 TW Ti:sapphire system at PALS facility and with proposed innovative scheme how to improve the injection of the electron bunch into the wake wave.

Chapter 3 concentrates on various methods how to convert a part of the electron energy into the electromagnetic radiation. Due to the author's participation on the grant project dedicated to betatron and Thompson/Compton source from laser plasma, the chapter is mostly focused on these two source. Nevertheless, other mechanisms as high harmonics generation and K-α radiation are mentioned.

As this study and intended further work is based almost exclusively on the numerical simulation, following chapter 4 presents numerical tools used, particle-in-cell method to simulate the laser-plasma interaction and further electron acceleration process, tracking of accelerated electrons and finally the method how to calculate the features of generated X-rays. The novel method to construct a spectrogram of X-ray pulse in wiggler regime of betatron radiation is presented.

Last chapter 5 discusses the results achieved up to now. Most of the attention is devoted to experimental campaign at PALS and to the impact of proposed injection scheme on generated x-rays with the use of the analysis tool introduced in previous chapter.

In this study, main attention is paid to the parts, where own research or implementation was carried out or where at least it is intended in the future. However, a lot of other topics was included for better understanding of this work and only a brief overview of these topics is offered. The references to the appropriate literature are always provided though.

Chapter 2

Laser Wakefield Acceleration

2.1 General overview

Laser wakefield acceleration (LWFA) is a method to accelerate electrons in laser plasma. The idea was originally suggested by Tajima and Dawson [Tajima and Dawson, 1979]. This concept may appear as counter-intuitive since the principle Lawson–Woodward theorem [Lawson et al., 1979, Mulser and Bauer, 2010] states that the net energy gain of a relativistic electron interacting with a continuous electromagnetic field in vacuum is zero. However, in this case it is not intended to accelerate electron by the laser beam itself, but rather by a plasma wake wave dragged by the laser beam propagating through the underdense plasma[1]. This structure can sustain large acceleration gradient of the order of hundreds GV/m for a sufficient time to accelerate electrons up to GeV energies in a several mm thick plasma layer. The conventional radiofrequency accelerators generate acceleration gradient in the order of tens of MV/m, so the large facilities with the size of the order of tens of meters are needed to obtain the same results. On the other hand, the advantages of the conventional accelerator still surpass such drawback, they are more stable, tunable and generate the monoenergetic electron bunches.

Several mechanism of the electron acceleration appeared and the features of the produced bunches are continuously improved. The state-of-the-art in 2009 is concluded by

[1] A laser beam with a wavelength λ_L can propagate in unmagnetized plasma if the plasma density is smaller than the critical electron plasma density n_c given by

$$n_c = \frac{\varepsilon_0 m_e c^2}{4\pi^2 e^2 \lambda_L^2}$$

which can be expressed in a practical units as

$$n_c\ [\mathrm{cm}^{-3}] = \frac{1.1 \times 10^{21}}{\lambda_L\ [\mu\mathrm{m}]}.$$

The critical density is such a density where $\omega_{p,e} = \omega_L$. If a plasma density is higher than the critical density, a laser beam is reflected from plasma.

Esarey [Esarey et al., 2009], more recent overview can be found in the book by Macchi [Macchi, 2013]. Recently, multi-GeV electrons have been generated using PW laser system [Wang et al., 2015, Leemans et al., 2015] by the LWFA mechanism.

In this study, only the non-linear cavitated wakefield regime will be introduced, since this regime is currently considered as a most efficient one. The concepts of ponderomotive force, plasma wave and ion cavity will be briefly introduced in the following sections. In the last section of this chapter, the mechanisms of optical injection of the electrons in the ion cavity will be reviewed.

2.2 Plasma wave induced by a ponderomotive force

The ponderomotive force is a non-linear force that charged particles experience in an inhomogeneous oscillating electric field, e.g. in the presence of the short intense laser pulse. It can be expressed as

$$\mathbf{F}_p = -\frac{q^2}{4m\omega_L^2}\nabla(\mathbf{E}^2), \tag{2.1}$$

where q is the electrical charge of the particle, m is its mass, ω_L is the angular frequency of the field oscillations, and $\mathbf{E}$ is the amplitude of the electric field. This force is associated with the intensity gradients of the laser pulse. It expels both ions and electrons out of high intensity region. Due to the high inertia of the heavy ions, they are not significantly influenced by ponderomotive force on very short interaction time, whereas the light electrons are driven away. Therefore a small charge density perturbation is present. Such charge density perturbation oscillates at characteristic frequency, the plasma frequency

$$\omega_p = \sqrt{\frac{n_e e^2}{m_e \varepsilon_0}}, \tag{2.2}$$

where n_e is electron density in plasma, e is electron charge, m_e is electron mass, and ε_0 is vacuum permittivity. These plasma oscillations are called plasma wave, because they are travelling behind the laser pulse. Consequently, as the laser pulse propagates deeper in the plasma, the plasma wave is dragged in the wake of the laser pulse. The phase velocity of the plasma wave is approximately equal to the laser pulse group velocity.

The intensity of laser pulse may be expressed in the form of the normalized vector potential defined as

$$\mathbf{a} = \frac{e\mathbf{A}}{m_e c}. \tag{2.3}$$

Let us define the amplitude of this normalized vector potential $\mathbf{a}$ as a laser strength parameter a_0. In practical units, a_0 is given as

$$a_0 = 0.855\sqrt{I_L\ [10^{18}\ \mathrm{W/cm^2}]}\lambda_L\ [\mu\mathrm{m}], \tag{2.4}$$

where I_L is the laser intensity and λ_L is the laser wavelength.

For the low intensity pulses with $a_0 \ll 1$, the formed plasma wave is linear. It has sinusoidal shape and propagates with the plasma frequency, i.e.

$$\phi(\mathbf{x}, t) = \phi_0(\mathbf{x}) \sin(\omega_p t), \tag{2.5}$$

where function ϕ represents scalar potential.

For higher intensities, non-linear effects are present. The electrons trapped in the plasma wave could be potentially accelerated by its fields.

2.3 Cavitated wakefield regime

The cavitated wakefield regime (bubble regime, blow-out regime) [Pukhov and Meyer-ter Vehn, 2002] is currently considered as the most efficient mechanism to accelerate electrons in a plasma wave. The plasma wave comprises of an ion cavity (bubble), i.e. the spherical region in the wake of the laser pulse, which contains only ions as the light electron were expelled by ponderomotive force, and following plasma oscillations.

This regime is achieved, when the following three conditions are fulfilled:

1. the waist size w_0 of the incident laser pulse is coupled with the plasma

$$\frac{\omega_p}{c} w_0 = 2\sqrt{a_0} \tag{2.6}$$

2. the pulse length τ is approximately the half of the plasma wavelength λ_p

$$c\tau \approx \frac{\lambda_p}{2} = \frac{\pi c}{\omega_p} \tag{2.7}$$

3. the laser intensity is sufficiently high

$$a_0 > 2. \tag{2.8}$$

A strong gradient of the electric field in the longitudinal direction with respect to the original laser beam direction is formed in this ion cavity. Electrons may be trapped in the rear part of the bubble and accelerated significantly. During the acceleration process, the trapped electrons advance to the middle of the ion cavity, since they propagate almost with the speed of light, whereas the ion cavity propagates slower, with the group velocity of the laser pulse in the plasma

$$v_g = c \left[1 - \frac{\omega_p^2}{2\omega_L^2} - \frac{2c^2}{(\omega_L w_0)^2} \right]. \tag{2.9}$$

Once the electrons reach the middle of the bubble, they experience inverse polarity of the electric field and therefore they are decelerated. The energy gain is proportional to the

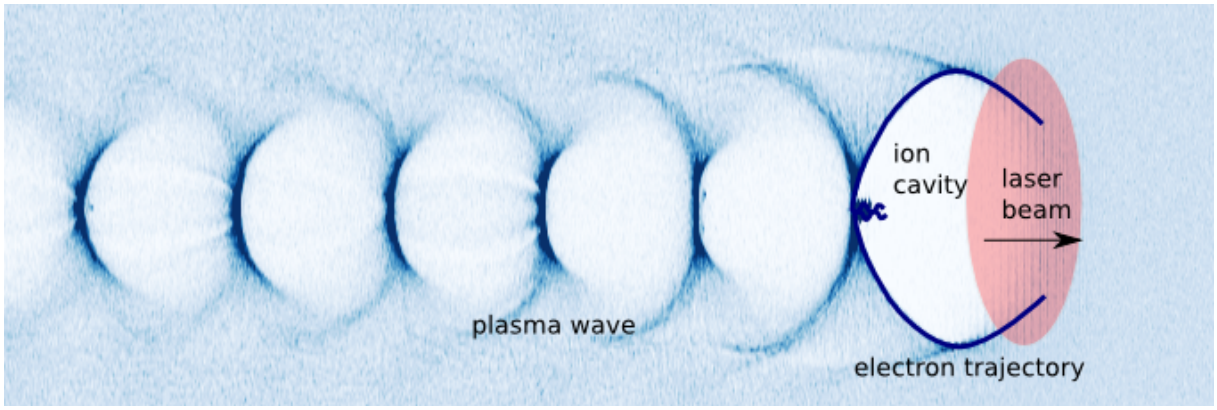

Figure 2.1: Scheme of the cavitated wakefield regime of the laser wakefield acceleration. Background is obtained from 3D PIC simulation and represents the electron density. The blue lines shows the trajectories of the self-injected electrons.

time spent in the rear part of the ion cavity. The distance travelled in the accelerating field is called the dephasing length.

The plasma frequency is proportional to the square root of the plasma density. It can be seen from the equation (2.9), that the ion cavity velocity drops with the increase of the electron density. It means that the electrons might be accelerated more in the less dense plasma. On the other hand, in the high density plasma the self-focusing effect sustains the high intensity of the laser pulse which drags the plasma wave. The threshold for the relativistic self-focusing is the relativistic critical power [Mourou et al., 2006]

$$P_{cr} = \frac{m_e^2 c^5 \omega_L^2}{e^2 \omega_p^2} \approx 17 \left(\frac{\omega}{\omega_p}\right)^2 \text{ GW}. \tag{2.10}$$

The ion cavity would fall apart if the self-focusing would not be present due to the diffraction of the laser light during its propagation in the plasma. The plasma density has to be chosen with respect to the laser parameters understanding both dephasing and self-focusing to efficiently accelerate the electrons in the cavitated wakefield regime of the laser wakefield acceleration.

Highly cited article about 3D simulations of the bubble regime of laser wakefield acceleration by the 5 – 25 TW lasers was written by Tsung [Tsung et al., 2006].

2.4 Optical injection

Quasimonoenergetic high energy electron beams (hundreds of MeV) can be generated by interaction of short (tens of fs) intense laser beam with gas target applying the following mechanism. The pump pulse generates the wakefield structure, whereas the injection pulse preheats the plasma in the way that electrons are trapped in the bubble. Although the simplest mechanism to inject the electron into an ion cavity is to let the nature to do

it by itself, this method called self-injection [Benedetti et al., 2013] has several significant downsides. The characteristic issue is the large fluctuation of the electron spectra. The single laser pulse is responsible for both the generation of the wake wave, and for the injection. The instability of pump laser power, gas density profile and other possible perturbations influence the features of generated beam distinctively.

One of the possibilities to stabilise the properties of produced electron beams is to separate the processes of wakefield generation and the injection of electron into this wakefield. Among other conceivable manners like tailoring the gas density profile or using the mixture of gases to provoke ionisation injection, an optical injection is an reasonable alternative.

In optical injection configuration, the pump pulse is responsible for the formation of the wake wave, and an additional injection pulse injects electron bunch in a controlled manner into an ion cavity.

This scheme was firstly proposed by Umstadter [Umstadter et al., 1996], both by analytical calculation and numerical simulation (PIC 1D3V). The use of orthogonally directed beams was suggested. The perpendicular polarisations of both beams were considered. The main idea of this concept was that the transverse ponderomotive force of the injection pulse would disturb electrons motion on their eight-like trajectories in their phase space [Petržílka et al., 2002] and pre-accelerate a considerable part of them in direction of the pump pulse propagation sufficiently. Consequently, these electrons were intended to be trapped and further accelerated in wake wave. The injection pulse was suggested to be even stronger than the pump pulse. For instance, the following example was presented. Whereas the intended laser strength parameter of the main pulse should have been $a_0 = 1.0$, the threshold value for the injection beam laser strength parameter was $b_0 \gtrsim 1.6$. The natural drawback is that such strong injection beam could potentially destroy the wakefield structure.

However, this pioneer work was performed in 1990's, when cavitated wakefield regime has not been yet discovered [Pukhov and Meyer-ter Vehn, 2002] and only the linear regime of laser wakefield acceleration was considered. Another big concern was connected with the possible issues related to the proper synchronization of both femtosecond pulses. Such a synchronisation was experimentally demonstrated though [Zhang et al., 2003].

Fubiani [Fubiani et al., 2004] and Kotaki [Kotaki et al., 2004] suggested independently injection by counter-propagating pulses with the same polarisation of both beams. This scheme was experimentally demonstrated as well [Faure et al., 2006], and the stable generation of collimated (5 mrad divergence), monoenergetic (with energy spread $\lesssim 10\%$), tunable (between 15 and 250 MeV) electron beams was reported. As the injection pulse is weak in comparison with the pump pulse, it does not perturb the wakefield structure noticeably. Nevertheless, injection pulse has to propagate through long plasma region

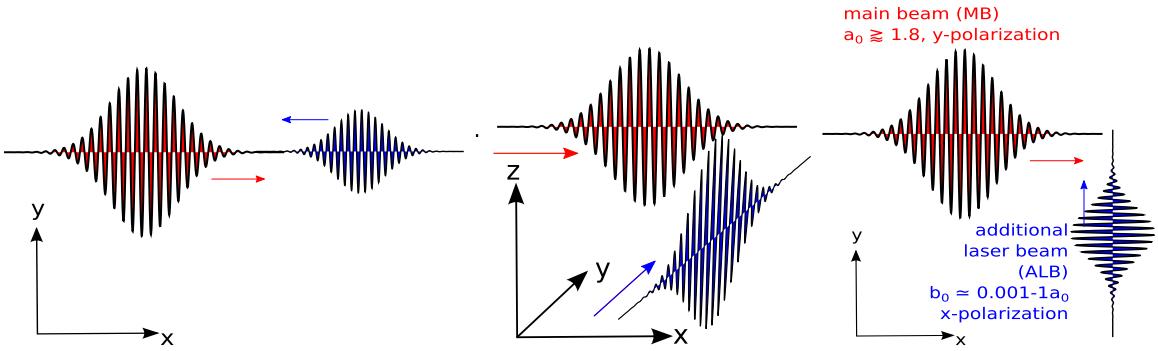

Figure 2.2: Discussed schemes of the optical injection. Left: Injection by counter-propagating laser beam introduced in [Fubiani et al., 2004]. Middle: Scheme proposed by Wang [Wang et al., 2008] using perpendicular main and injection pulses with parallel polarisations. Right: Proposed scheme using perpendicular main and injection pulses with transverse polarisations.

before collision with the pump pulse and due to its low intensity it is susceptible to defocusing. The scheme with counter-propagating injection and pump beams is investigated and improved also nowadays, an overview of the state-of art is given dissertation [Lehe, 2014].

Lehe discusses that in the time of the collision of the counter-propagating laser pulses a beat wave forms. Longitudinal ponderomotive force pushes electrons of the local intensity maxima. These electrons can be dephased with respect to the wakefield and trapped. This mechanism is called cold optical injection [Davoine et al., 2010]. Total ponderomotive force may induce an additional effect though. Electrons can experience stochastic heating in the modulated intensity pattern. This effect is the same as the one discussed in by the original work of Umstadter [Umstadter et al., 1996]. Electron may gain momentum and therefore be preaccelerated and subsequently trapped in the wake wave dragged by the pump pulse. This mechanism is called warm optical injection.

Wang [Wang et al., 2008] returned the attention back to the perpendicular pulses. He chose configuration with the same polarisation perpendicular to the plane formed by two pulses. An additional third pulse following the pump pulse destroys the wake wave and suppresses self-injection hereby. The argumentation is presented for the linear regime of laser wakefield acceleration with $a_0 \approx 1.5$. Although the original Umstadter proposal [Umstadter et al., 1996] with perpendicularly polarised beams was mentioned, the comparison of those two cases was not carried out or even discussed.

Both of the schemes with the orthogonally directed pulses [Umstadter et al., 1996, Wang et al., 2008] operated in the linear regime, partly because the state-of-the-art of the laser technique in the past, but mainly to avoid the self-injection of the electrons in the case of the cavitated wakefield regime.

As a part of this study, a certain redesign of the original proposal of the optical

injection by orthogonally directed and perpendicularly polarized laser beams is studied and compared with other introduced concepts. This redesign reacts on the progress in the laser technology and physical understanding. The proposed scheme can operate on highly non-linear regime of LWFA ($a_0 > 2$ and even higher) and the injection pulse is supposed to be very weak in comparison with the pump pulse $b_0 \sim 0.1a_0$ to avoid its disturbing effect on the dynamics of the ion cavity.

Moreover, as the large intensity of the pump pulse is assumed, there is no requirement of high plasma density to make use of the self-focusing of the laser beam to sustain sufficient intensity and the wakefield structure. As the time when self-injection occurs increases with the decreasing plasma density, the acceleration of the optically injected bunch may take places well before self-injection occurs. Mechanisms to sort out the lower energy electrons by filtering them with the magnetic field [Umstadter et al., 1996] or by using the slightly delayed laser pulse [Wang et al., 2008] may be still applied.

The suggested optical injection mechanisms are depicted in Figure 2.2. The comparison between these cases and their impact on generated X-rays are presented in Chapter 5.

2.5 Ionisation injection

Another convenient mechanism to trap the electrons in the wake wave is an ionisation injection [Pak et al., 2010]. A mixture of two gases is used, typically the dominant part of the mixture are light elements and the trace amount of the heavier elements is added (e.g. 99 % of He + 1 % of Ar as in the experiment at PALS). The heavier elements have typically a huge gap between ionisation potentials (e.g. for argon 143.5 eV is needed to ionise it 8 times and 422 eV to ionise it 9 times). The power of the laser pulse is kept under third of the critical power (2.10) to suppress the self-injection when using this scheme. Therefore such a scheme is suitable even for low power laser systems ($\lesssim$ 10 TW).

Electrons are injected to the wakefield due to the tunnel ionisation of the inner K-shell electrons which occurs only in the region of very high intensity, i.e. close to the focus. The significant amount of the energy of the laser pulse is consumed to the ionisation of gas. Therefore the ionisation process is well spatially and temporally localised (in the case of lower intensity), and it results in short quasimonoenergetic electron beams generation.

Experiment performed at PALS laboratory, which is described in Section 5.1, is based on slightly modified version of ionisation injection. It could be rather called injection induced by ionisation. Due to the high plasma density used and higher laser power the relativistic self-focusing sustains high laser intensity for a longer time. It means that the field ionisation takes place for a longer time during the acceleration process. Quasimonochromacity and length of the bunch are therefore compromised.

Chapter 3

X-Rays from Laser Plasma

Once the accelerated electron bunch is generated via LWFA mechanism, part of its energy can be converted into X-rays. Several mechanisms are reviewed. Great overview of considered sources of X-ray radiation proposes the article [Corde et al., 2013]. However, the theory of the radiation emitted by a moving charge is introduced at the beginning of this chapter.

3.1 Radiation by a moving charge

Theory of electrodynamics [Landau and Lifshitz, 1951, Jackson, 1999] states that an accelerated moving charge emits the electromagnetic radiation. The change of the propagation direction of this moving charge is considered as acceleration too. Hence, high energy moving charge could radiate high energy electromagnetic radiation (X-rays) when its motion is properly tailored.

The problem of radiation of electromagnetic waves by single charged moving particle has been firstly formulated by Liénard and Wiechert, independently of each other, even before formulation of special theory of relativity. In non-relativistic regime, the radiation power only depends on the acceleration of charged particles. However, in relativistic limit as the particle velocity $v = |\mathbf{v}|$ is comparable to the speed of light in vacuum c, radiation power increases rapidly and radiation is emitted especially on the axis in the direction of propagation with the angular spread $\theta = 1/\gamma$, where $\gamma = 1/\sqrt{1-\boldsymbol{\beta}^2}$ is the Lorentz factor and $\boldsymbol{\beta} = \mathbf{v}/c$ is dimensionless velocity.

The properties of radiation are interconnected with the electron trajectory. Retarded potentials [1] of a moving electron can be derived directly from the Maxwell's equations

[1] Liénard-Wiechert potentials, formulated in 1898.

and are given as [Jackson, 1999]

$$\begin{aligned}\Phi(\mathbf{r},t) &= \frac{e}{4\pi\varepsilon_0}\frac{1}{R(t')(1-\mathbf{n}(t')\cdot\boldsymbol{\beta}(t'))}\\ \mathbf{A}(\mathbf{r},t) &= \frac{e}{4\pi\varepsilon_0 c}\frac{\boldsymbol{\beta}(t')}{R(t')(1-\mathbf{n}(t')\cdot\boldsymbol{\beta}(t'))}\end{aligned} \tag{3.1}$$

where $R(t') = |\mathbf{r} - \mathbf{r_p}(t')|$ is the distance between the point of emission and observer, $\mathbf{r_p}$ is the position of radiating charge, $\mathbf{n}$ is the unit vector in direction of $\mathbf{r} - \mathbf{r_p}$. Consider that the vectors $\mathbf{r_p}$, $\mathbf{n}$ and $\boldsymbol{\beta}$ are expressed in the retarded time t'. The retarded time is the time when the field began to propagate from the point where it was emitted $\mathbf{r_p}$ to the observer who is located in point $\mathbf{r}$. The relation between the retarded time t' and observer's time t is

$$t' = t - \frac{|\mathbf{r} - \mathbf{r_p}|}{c}. \tag{3.2}$$

It is worth mentioning that in non-relativistic limit when $\beta \ll 1$ the potentials 3.1 take shape of classical scalar and vector potentials.

Associated electric and magnetic field can be obtained from

$$\begin{aligned}\mathbf{E} &= -\nabla\Phi - \frac{\partial\mathbf{A}}{\partial t},\\ \mathbf{B} &= \nabla\times\mathbf{A},\end{aligned} \tag{3.3}$$

where spatial and time derivatives pertain to $\mathbf{r}$ and t (observing location and time). However, electric and magnetic field is usually written in the retarded time t'. To be able to perform such a transformation, relation between observer's and retarded time (3.2) has to be differentiated, i.e.

$$\frac{\mathrm{d}t}{\mathrm{d}t'} = 1 - \mathbf{n}(t')\cdot\boldsymbol{\beta}(t'). \tag{3.4}$$

Combining with the formulas for potentials (3.1), electromagnetic field emitted by relativistic moving charge if found

$$\begin{aligned}\mathbf{E}(\mathbf{r},t) &= \frac{e}{4\pi\varepsilon_0}\left\{\frac{(1-\boldsymbol{\beta}^2)(\mathbf{n}-\boldsymbol{\beta})}{R^2(1-\mathbf{n}\cdot\boldsymbol{\beta})^3} + \frac{\mathbf{n}\times[(\mathbf{n}-\boldsymbol{\beta})\times\dot{\boldsymbol{\beta}}]}{cR(1-\boldsymbol{\beta}\cdot\mathbf{n})^3}\right\}_{ret}\\ \mathbf{B}(\mathbf{r},t) &= \frac{e}{4\pi\varepsilon_0 c}\left\{\frac{(1-\boldsymbol{\beta}^2)[\mathbf{n}\times(\mathbf{n}-\boldsymbol{\beta})]}{R^2(1-\mathbf{n}\cdot\boldsymbol{\beta})^3} + \frac{\mathbf{n}\times\dot{\boldsymbol{\beta}}+\mathbf{n}\times[\mathbf{n}\times(\boldsymbol{\beta}\times\dot{\boldsymbol{\beta}})]}{cR(1-\boldsymbol{\beta}\cdot\mathbf{n})^3}\right\}_{ret}\\ &= \frac{1}{c}[\mathbf{n}\times\mathbf{E}]_{ret}.\end{aligned} \tag{3.5}$$

Indices *ret* mean that vector quantities $\mathbf{r_p}$, $\mathbf{n}$, $\boldsymbol{\beta}$ and $\dot{\boldsymbol{\beta}} = \mathrm{d}\boldsymbol{\beta}/\mathrm{d}t$ are evaluated in retarded time introduced in (3.2). More proper derivation can be found in [Jackson, 1999] and even in various courses of electrodynamics, e.g. in [Hirose, 2011]. First terms in braces are so called *velocity fields* which are independent on acceleration, second ones are *acceleration fields*, which depend linearly on $\dot{\boldsymbol{\beta}}$. Velocity fields are static Coulomb fields falling of as

$|\mathbf{r}-\mathbf{r_p}|^{-2}$, acceleration fields decrease with $|\mathbf{r}-\mathbf{r_p}|^{-1}$. Velocity fields can be omitted in the case of this work, as we are only interested in radiation in the far field.

Let us introduce a Poynting's vector as

$$\mathbf{S} = \mathbf{E} \times \mathbf{H} = \frac{1}{\mu_0}\mathbf{E} \times \mathbf{B}, \tag{3.6}$$

because the vacuum is a sufficient approximation for our underdense plasma, especially when the emitted electromagnetic waves are x-rays. After substitution from the last relation in equations (3.5) and usage of the *bac minus cab* rule from vector calculus we obtain

$$\mathbf{S} = \frac{1}{\mu_0 c}\mathbf{E} \times (\mathbf{n} \times \mathbf{E}) = \frac{1}{\mu_0 c}\left[\mathbf{n}|\mathbf{E}|^2 - \mathbf{E}(\mathbf{E}\cdot\mathbf{n})\right]_{ret}. \tag{3.7}$$

Let us omit the first Coulomb term in the equation for the electric field in (3.5) and substitute this relation into (3.7). The second term in (3.7) vanishes in our case and we can write the radial component of the Poynting vector as

$$\mathbf{S}\cdot\mathbf{n} = \frac{e^2}{16\pi^2\varepsilon_0 c}\left|\frac{\mathbf{n}\times[(\mathbf{n}-\boldsymbol{\beta})\times\dot{\boldsymbol{\beta}}]}{R(1-\mathbf{n}\cdot\boldsymbol{\beta})^3}\right|^2_{ret}. \tag{3.8}$$

Two observations can be underlined; firstly, the angular distribution of the emitted radiation is determined by the relationship between observation direction $\mathbf{n}$ and electron velocity $\boldsymbol{\beta}$ and acceleration $\dot{\boldsymbol{\beta}}$. Furthermore, the strong dependence on the factor $(1-\mathbf{n}\cdot\boldsymbol{\beta})$ causes that only forward directional beam is produced in the ultrarelativistic case.

We can understand the quantity $[\mathbf{S}\cdot\mathbf{n}]_{ret}$ as an energy per unit area per unit time detected at an observation point at time t of radiation emitted in the retarded time t'. Based on this observation, radiated power per unit solid angle can be defined as

$$\frac{\mathrm{d}P}{\mathrm{d}\Omega} = R^2(\mathbf{S}\cdot\mathbf{n})\frac{\mathrm{d}t}{\mathrm{d}t'} = R^2(\mathbf{S}\cdot\mathbf{n})(1-\boldsymbol{\beta}\cdot\mathbf{n}) \tag{3.9}$$

and from the equation (3.8) it is found that

$$\frac{\mathrm{d}P}{\mathrm{d}\Omega} = \frac{e^2}{16\pi^2\varepsilon_0 c}\frac{\left|\mathbf{n}\times[(\mathbf{n}-\boldsymbol{\beta})\times\dot{\boldsymbol{\beta}}]\right|^2}{(1-\mathbf{n}\cdot\boldsymbol{\beta})^5}. \tag{3.10}$$

The energy radiated per solid angle is

$$\frac{\mathrm{d}\mathcal{E}}{\mathrm{d}\Omega} = \int_{-\infty}^{+\infty}\frac{\mathrm{d}P}{\mathrm{d}\Omega}\mathrm{d}t \tag{3.11}$$

and after substitution of the acceleration term of electric field from (3.5) into (3.10) we can write

$$\frac{\mathrm{d}\mathcal{E}}{\mathrm{d}\Omega} = c\varepsilon_0\int_{-\infty}^{+\infty}|R\mathbf{E}|^2\mathrm{d}t. \tag{3.12}$$

Let us introduce the Fourier transform as

$$F(\omega) = \mathfrak{F}[f(t)](\omega) = \int_{-\infty}^{+\infty} f(t)\mathrm{e}^{i\omega t}\mathrm{d}t \tag{3.13}$$

and inverse Fourier transform as

$$f(t) = \mathfrak{F}^{-1}[F(\omega)](t) = \frac{1}{2\pi}\int_{-\infty}^{+\infty} F(\omega)\mathrm{e}^{-i\omega t}\mathrm{d}t. \tag{3.14}$$

In this case, Parseval's theorem takes the form

$$\int_{-\infty}^{+\infty} |f(t)|^2\mathrm{d}t = \frac{1}{2\pi}\int_{-\infty}^{+\infty} |F(\omega)|^2\mathrm{d}\omega \tag{3.15}$$

and we can rewrite the formula for emitted energy (3.12) as

$$\frac{\mathrm{d}\mathcal{E}}{\mathrm{d}\Omega} = \frac{c\varepsilon_0}{2\pi}\int_{-\infty}^{+\infty} \left|\mathfrak{F}[R(t)\mathbf{E}(t)](\omega)\right|^2 \mathrm{d}\omega = \frac{c\varepsilon_0}{\pi}\int_{0}^{+\infty} \left|\mathfrak{F}[R(t)\mathbf{E}(t)](\omega)\right|^2 \mathrm{d}\omega. \tag{3.16}$$

The radiated energy per solid angle can be related to the integral of the frequency spectrum

$$\frac{\mathrm{d}\mathcal{E}}{\mathrm{d}\Omega} = \int_0^{+\infty} \frac{\mathrm{d}^2 I}{\mathrm{d}\omega\mathrm{d}\Omega}\mathrm{d}\omega, \tag{3.17}$$

and the formula for the frequency and the angular distribution of the radiation emitted by the moving charge is

$$\frac{\mathrm{d}^2 I}{\mathrm{d}\omega\mathrm{d}\Omega} = \frac{c\varepsilon_0}{\pi}\left|\mathfrak{F}[R(t)\mathbf{E}(t)](\omega)\right|^2. \tag{3.18}$$

The task to investigate the properties of the radition emitted by a moving charge was reformulated as the calculation of the Fourier transform of the electric field generated by the charge. This electric field depends according to equation (3.5) only on the trajectory of the moving charge.

By substituting the formula for electric field (3.5) into (3.18) it can be written that

$$\frac{\mathrm{d}^2 I}{\mathrm{d}\omega\mathrm{d}\Omega} = \frac{c\varepsilon_0}{\pi}\left|\int_{-\infty}^{+\infty} \frac{e}{4\pi\varepsilon_0}\left[R\,\frac{\mathbf{n}\times[(\mathbf{n}-\boldsymbol{\beta})\times\dot{\boldsymbol{\beta}}]}{cR(1-\mathbf{n}\cdot\boldsymbol{\beta})^3}\right]_{ret} \mathrm{e}^{i\omega t}\mathrm{d}t\right|^2, \tag{3.19}$$

where $t = t' + \mathbf{n}\cdot\mathbf{R}(t')/c$ and by changing the integration variable from t to t' we finally obtain the formula for the radiation emitted by moving charge as

$$\frac{\mathrm{d}^2 I}{\mathrm{d}\omega\mathrm{d}\Omega} = \frac{q^2}{16\pi^3\varepsilon_0 c}\times\left|\int_{-\infty}^{\infty} \exp\left(i\omega\left[t' - \frac{\mathbf{n}\cdot\mathbf{R}(t')}{c}\right]\right)\times\frac{\mathbf{n}\times[(\mathbf{n}-\boldsymbol{\beta})\times\dot{\boldsymbol{\beta}}]}{(1-\boldsymbol{\beta}\cdot\mathbf{n})^2}\mathrm{d}t'\right|^2. \tag{3.20}$$

Such a major formula deserves at least a brief discussion. Let us pinpoint several observations:

1. Moving charge radiates only when is accelerated (it means that it is accelerated, decelerated or its motion direction is changing).

2. Radiated energy is maximum when $\boldsymbol{\beta}\cdot\mathbf{n} \longrightarrow 1$, so in the case when $\beta \approx 1$ and $\boldsymbol{\beta} \parallel \mathbf{n}$. It means that relativistic electron radiates by orders of magnitude more intense than non-relativistic one and that the radiation is highly directional along the direction of its velocity.

3. Radiated energy increases with the square of the acceleration $\dot{\boldsymbol{\beta}}$.

4. The goal for X-rays generation from the relativistic electrons is to force the transverse motion of accelerated electrons. This is the principle of standard undulators and wigglers and plasma based sources are based on this fact as well.

Up to this point, radiation only of a single electron was investigated. If the incoherent electron bunch is comprised of N_e electrons, which are randomly distributed inside the bunch, then the total radiation is simply a sum of the contributions of single electrons and can be estimated as N_e times a radiation emitted by typical electron

$$\frac{\mathrm{d}^2 I}{\mathrm{d}\omega \mathrm{d}\Omega} = \sum_{i=1}^{N_e} \frac{\mathrm{d}^2 I_i}{\mathrm{d}\omega \mathrm{d}\Omega} \approx N_e \left.\frac{\mathrm{d}^2 I}{\mathrm{d}\omega \mathrm{d}\Omega}\right|_{ave}. \tag{3.21}$$

In large accelerators or in laser-plasma accelerators, this condition is fulfilled.

Proper analysis performed in [Jackson, 1999] leads to the formula for the temporal evolution of the radiating power per unit frequency. It can be written in SI units as [Corde et al., 2013]

$$\frac{\mathrm{d}P}{\mathrm{d}\omega}(t) = \frac{\sqrt{3}q^2}{12\pi^2\varepsilon_0 c}\frac{\omega}{\gamma^2}\int_{\omega/\omega_c}^{\infty} K_{5/3}(\xi)\mathrm{d}\xi, \tag{3.22}$$

where

$$\omega_c = \frac{3\gamma^3 c}{2\rho} \tag{3.23}$$

is critical frequency, ρ is the instantaneous radius of curvature[2] and $K_{5/3}$ is the modified Bessel function of the second kind.

Temporal evolution of the radiated power can be obtained as

$$P(t) = \int_0^{+\infty} \frac{\mathrm{d}\,P}{\mathrm{d}\omega}(t)\mathrm{d}\omega = \frac{2e^2\omega_c^2}{17\pi\varepsilon_0 c\gamma^2}, \tag{3.24}$$

total energy radiated by moving charge is

$$\mathcal{E} = \int_{t_1}^{t_2} P(t)\mathrm{d}\,t = \int_{t_1}^{t_2}\int_0^{+\infty} \frac{\mathrm{d}\,P}{\mathrm{d}\,\omega}(t)\,\mathrm{d}\omega\mathrm{d}t. \tag{3.25}$$

The figure 3.1 shows the radiation of typical electron during its acceleration and also deceleration phases. Its trajectory was taken from PIC simulation of the laser wakefield acceleration. It includes evolution of its energy and its transverse coordinate. Radiated

[2] If we have curve described in the Cartesian coordinates as $y = y(x)$, than radius of curvature is

$$\rho = \left|\frac{(1+y'^2)^{3/2}}{y''}\right|.$$

If the curve is described parametrically by functions $x = x(t)$ and $y = y(t)$, than radius of curvature is

$$\rho = \left|\frac{(\dot{x}^2+\dot{y}^2)^{3/2}}{\dot{x}\ddot{y}-\dot{y}\ddot{x}}\right|.$$

power was calculated according to the formula (3.22). Characteristics of its radiation are linked with its trajectory. For instance, electron radiates the most when it reaches the turning points of its betatron oscillations. Furthermore, it almost does not radiate when passing its central position. The energy of radiation strongly depends on electron energy.

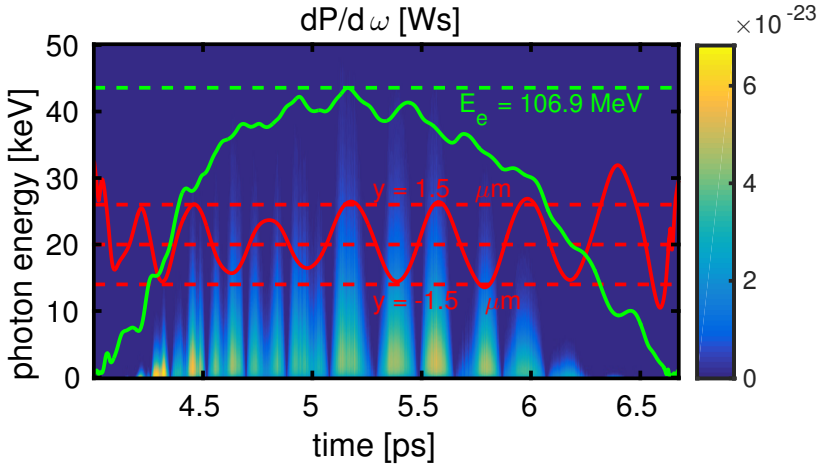

Figure 3.1: Radiation of example electron from PIC simulation during its acceleration and also deceleration process. Its oscillations in transverse direction (red) and evolution of its energy (green) are schematically represented. Electron radiates at the most in its turning points. Energy of radiation strongly depends on electron energy.

This example electron was accelerated up to 107 MeV, amplitude of its betatron oscillations reached 1.56 μm at that time. The radiated energy of 4.53 keV is obtained from equation (3.25). Critical energy of radiation averaged over time was 5.50 keV, according to the equation (3.23). It can be interpreted that this electron emitted 0.82 photons at the critical energy. Such an observation is in the good agreement with the theoretical predictions [Corde et al., 2013].

The length of X-ray bunch Δt radiated by single electron observed in the far field on the axis can be calculated. Let us consider that the radiation begins in the time t_1 and ends in the time t_2. Hence, the time delay which gained radiating electron up to the time t_2 compared to the photon radiated in the time t_1 can be written as

$$\Delta t \approx \frac{\int_{t_1}^{t_2}(c - v_x(t))\mathrm{d}t}{c}, \tag{3.26}$$

since $v_x \approx c$, where v_x is the velocity of the electron in the longitudinal direction. In this case, when $t_1 \approx 4.45$ ps and $t_2 = 5.95$ ps as can be seen from the figure, the length of the radiation is 2.23 fs (proper values of longitudinal electron velocity has been substituted into the equation (3.26)). Therefore, the length of the X-ray bunch generated by all trapped electrons depends mainly on the length of the injected electron bunch. In principle, X-ray pulses even shorter than laser pulse length can be generated.

3.2 Considered X-rays sources

3.2.1 K-α radiation

When laser with the intensity of the order of 10^{16} W/cm^2 irradiates the solid target, the plasma is created in the interaction region and expands back to the vacuum. Mechanism like resonance absorption, vacuum heating and $\mathbf{j} \times \mathbf{B}$ heating lead to the generation of hot electrons (their energy is of the order of tens or hundreds of keV, i.e. much higher that the energy corresponding to the plasma temperature). The hot electrons penetrate into the cold part of the target, and it results among other effects in the ionisations of the inner shells of atoms. As the relaxation periods of the ionised atoms with missing electron in the inner shell are very short, the atoms immediately proceed to the state with lower energy by two possible physical processes considered.

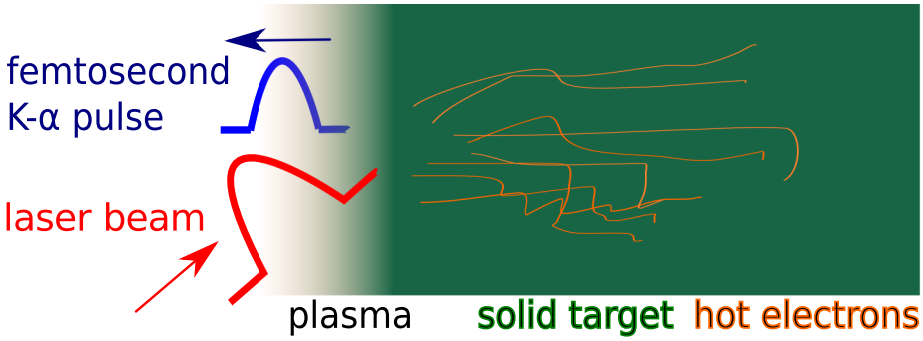

Figure 3.2: Scheme of K-α radiation source.

Firstly, the atom from a higher shell can jump down into the empty inner shell. The energy released is carried away by another electron from the outer shell as its kinetic energy. This mechanism is called Auger effect and occurs rather by low Z elements. No radiation is emitted.

Second mechanism leads to the photon emission. The characteristic radiation is induced by the drop of the electron to the empty inner shell connected with the emission of the well defined amount of energy in the form of photon.

Individual electron shells are marked with Latin letters K, L, M etc. and depth of the drop is marked with the Greek letter α, β etc. The symbol K-α means that electron drops to the most inner K shell from the closest L shell. The typical energies of K-α lines are in order of keV (e.g. 1.49 keV for aluminum, 8.02 keV for copper, and 22.0 keV for silver).

Characteristic radiation has discrete line spectrum and positions of lines are unique for every individual chemical element. The disadvantage of the K-α sources is that the radiation is emitted to the angle of 4π steradians. Additionally, significant part of the radiation is absorbed even before it leaves the solid target.

The topic was investigated in author's master thesis [Horný, 2014] and the phenomenon of the hot electron refluxing and its possible influence on K-α radiation was discussed in [Horný and Klimo, 2015].

3.2.2 High order harmonics radiation

High harmonic generation (HHG) is another process during which a target is illuminated by an intense laser pulse. Laser intensities are typically of the order of 10^{14} W/cm^2. Under such conditions, the sample will emit the high harmonics of the generation beam, typically up to the energy of hundreds of eV or units of keV. The spectrum is comprised of the individual harmonics. It can be divided into three parts:

1. the region of lower harmonics with their high intensity
2. plateau region where the intensities of neighbour harmonics are similar
3. and the high intensity region where the intensity of individual harmonics with the increasing harmonic number rapidly drops up to the position called harmonic cut-off.

HHG source provides tunable table top source of the radiation on the border between extreme ultraviolet light and soft X-rays. The harmonic cut-off varies linearly with increasing laser intensity up to certain the saturation intensity. High harmonics generation is are used in the generation of the attosecond pulses as well [Paul et al., 2001]. The overview of the high harmonics generation physics is given in [Schultz and Vrakking, 2013].

3.2.3 Betatron radiation

Betatron radiation is inherently connected with the the cavitated wakefield regime of the laser wakefield acceleration. Plasma cavity itself acts as a wiggler during the acceleration process. Electrons therefore perform transverse oscillation in addition to their acceleration in the longitudinal direction. Since their energy is relativistic, X-rays are emitted. The betatron radiation mechanism was proposed and firstly demonstrated independently by Kisilev [Kiselev et al., 2004] and Rousse [Rousse et al., 2004] in 2004.

Two regimes of the radiation with very different features can be distinguished, based on the relation between amplitude of betatron oscillation and betatron wavelength $\lambda_\beta \approx \frac{2\pi c}{\omega_\beta}$. According to the model introduced by Lu [Lu et al., 2007], the frequency of the transverse oscillations (betatron frequency) is given as

$$\omega_\beta = \frac{\omega_p}{\sqrt{2\gamma}} \tag{3.27}$$

and the amplitude of the betatron oscillations is proportional to $r_\beta \sim \gamma^{-1/4}$. The two regimes are depicted in Figure 3.3. The angle Ψ is defined as the maximal angle between

the electron trajectory and longitudinal axis. The fundamental parameter separating two regimes is generally marked as K and given as

$$K = \Psi\gamma. \tag{3.28}$$

In practical units, K parameter can be expressed as

$$K = 1.33 \times 10^{-10}\sqrt{\gamma n_e\ [\mathrm{cm}^{-3}]}r_\beta\ [\mu\mathrm{m}]. \tag{3.29}$$

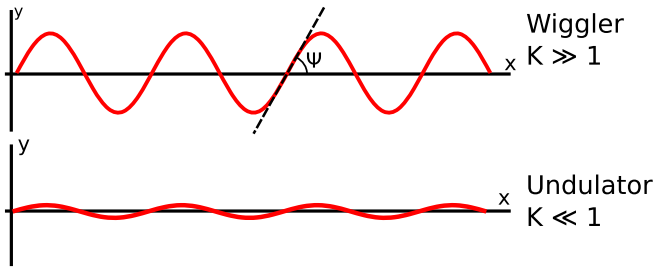

Figure 3.3: Undulator and wiggler regimes.

The wiggler regime with $K \gg 1$ is characterised by the fact that during the different stages of one betatron period electron radiates in different directions. As we already know from the equation (3.20), the electron radiates mainly when its differentiation of the acceleration $\dot{\boldsymbol{\beta}}$ is maximal, i.e. it the peaks of its trajectory. Hence, the observer on the axis receives bursts of radiation separated by a time $\lambda_\beta/2c$. The observer out of axis observes less energetic radiation bursts separated by a time λ_β/c. The duration of the one burst is

$$\tau = \frac{13\rho}{24\gamma^3 c} \approx \frac{1}{\omega_c}. \tag{3.30}$$

The radiation cone angle is $\Delta\theta = K/\gamma^2$, which is greater than $1/\gamma$. The radiated spectrum is comprised of many harmonics up to the critical frequency ω_c which can be written in practical units as

$$h\omega_c\ [\mathrm{eV}] = 5.24 \times 10^{-21}\gamma^2 n_e[\mathrm{cm}^{-3}]r_\beta[\mu\mathrm{m}] \tag{3.31}$$

The undulator regime occurs when $K \ll 1$, or alternatively when the angle Ψ is very low. The electron radiated exclusively in the longitudinal direction. The continuous profile of emitted radiation is observed. The radiated spectrum comprises of only several fundamental frequencies, thus it is quasimonoenergetic. The radiation cone angle is $\Delta\theta = 1/\gamma$.

The figure 3.4 presents example trajectories of the electrons trapped into the ion cavity performing betatron oscillations. The betatron wavelength ω_β is typically 400 µm in this case, whereas betatron amplitude is around 2 µm. However, it is still the wiggler regime.

Influence of direct laser acceleration on spectrum of betatron radiation from LWFA is currently being extensively discussed [Li et al., 2016, Shaw et al., 2016]. However, it

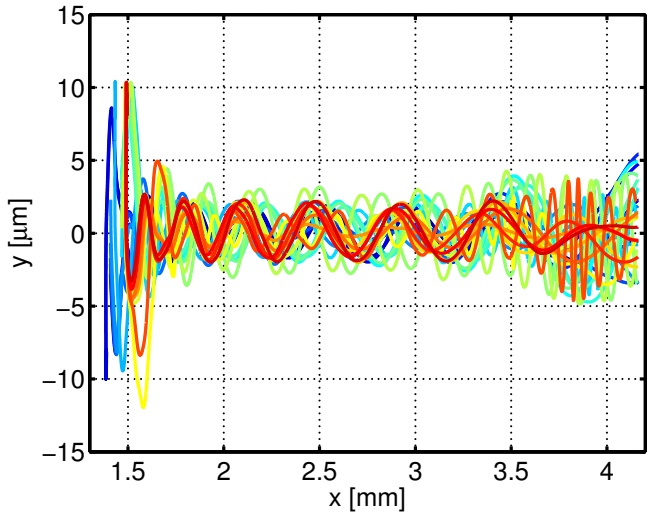

Figure 3.4: Example trajectories of the trapped electron trajectories from the PIC simulation.

seems that such phenomenon plays only minor role in the early stages of the acceleration process and therefore it can be omitted in the simulations carried out in this study.

3.2.4 Thomson scattering or the inverse Compton effect

The femtosecond X-ray pulses can be also produced from electrons oscillating in the field of an electromagnetic wave. The responsible physical phenomenon is the inverse Compton effect. The energetic electron transverses part of its energy to low energy photon of the laser wave. The inverse Compton effect is the view of quantum electrodynamics means the absorption of one or several photons by an electron with inherently following emission of one energetic photon. In the case, when photon energy is much lower than the mass energy of the particle in the rest frame $\hbar\omega \ll mc^2$, the mechanism is called Thomson scattering. Thomson scattering can be considered as the low energy limit of Compton scattering.

Two X-ray sources based on Thomson scattering will be introduced. The first one is a nonlinear Thomson scattering. This mechanisms is very simple. Electrons are initially at rest. A high intensity laser pulse with $a_0 \gg 1$ wiggles electrons, they performs highly nonlinear motion and emitted radiation consists of many harmonics. However, the generation of X-rays in the keV region requires intense laser pulse with $a_0 > 10$.

The K parameter is in this case

$$K \approx \frac{a_0}{\sqrt{2}} \tag{3.32}$$

and critical energy of radiation is

$$\hbar\omega_c = 0.3\frac{a_0^3}{\lambda_L\ [\mu\mathrm{m}]}. \tag{3.33}$$

Second mechanism is slightly more complicated, but on the other hand more promising. In Thomson backscattering configuration, electron are accelerated by LWFA and subsequently wiggled by the counter-propagating laser wave. This scheme was proposed already in 1963 [Arutyunian and Tumanian, 1963, Milburn, 1963]. Two laser beams are considered. The first one drives the laser wakefield accelerator, second one is responsible for scattering of the accelerated electrons.

The K parameter is in this case

$$K = a_0, \tag{3.34}$$

where a_0 is laser strength parameter of the second pulse. The mean energy of generated hard X-ray or γ photons can be estimated as

$$E_{ph} = 4\gamma_e^2 \hbar \omega_L f(a_0), \tag{3.35}$$

where $f(a_0) \approx 1$ for $a_0 \ll 1$ and $f(a_0) \approx a_0$ for $a_0 \geq 1$ [Corde et al., 2013].

For example, 500 MeV electrons colliding with laser beam with $a_0 = 2$ may generate 18 MeV photons [Sarri et al., 2014].

The idea of the Thomson back-scattering was rapidly simplified [Ta Phuoc et al., 2012] using the plasma mirror to reflect the laser pulse which drives the laser wakefield accelerator. The plasma mirror is realised by a foil placed orthogonally to the axis of laser beam propagation in the place, where the trapped electrons are already sufficiently accelerated. Reflected laser pulse makes the electrons oscillate and therefore emit X-rays via Thomson back-scattering mechanism.

Chapter 4

Numerical simulations

4.1 PIC algorithm

Particle-in-cell (PIC) method is a numerical method for integration of a certain class of the partial differential equations. It is used mainly in the plasma physics. Since its formulation in 1950's and 1960's [Harlow, 1964] it is being used as a mighty tool to simulate various physical effects in plasmas.

The method is based on the integration of Maxwell's equations and the motion equations for the particles. Maxwell's equations describe how the charges generate electromagnetic fields, equations of motion solve the impact of the electromagnetic fields on the particles. Rigorous derivation can be found in [Birdsall and Langdon, 2004]. Only a brief overview is presented here. Detailed explanation of the PIC method may be found among others in [Jaroszynski et al., 2009, Lehe, 2014, Markidis and Lapenta, 2011].

4.1.1 Physical background and numerical implementation

Plasma as quasineutral system is comprised of charged and neutral particles. Charged particles interact with each other, the force describing this interaction is the Lorentz force. This force can be written for very particle marked with the index p

$$\mathbf{F}_p = q_p[\mathbf{E}(\mathbf{x}_p) + \mathbf{v}_p \times \mathbf{B}(\mathbf{x}_p)], \tag{4.1}$$

where q_p is charge of p-th particle, $\mathbf{x}_p$ its position and $\mathbf{E}$ and $\mathbf{B}$ electric and magnetic fields. Lorentz force is calculated from the knowledge of the electric and magnetic field in the places where the simulated particles are located. Electric and magnetic field are generated partly by the particles in the system themselves, partly by external sources,

e.g. by laser beam. Maxwell's equations for these fields are

$$\nabla \cdot \mathbf{E} = \frac{\rho}{\varepsilon_0} \tag{4.2}$$

$$\nabla \times \mathbf{E} = -\frac{\partial \mathbf{B}}{\partial t} \tag{4.3}$$

$$\nabla \cdot \mathbf{B} = 0 \tag{4.4}$$

$$\nabla \times \mathbf{B} = \mu_0 \mathbf{j} + \mu_0 \varepsilon_0 \frac{\partial \mathbf{E}}{\partial t}, \tag{4.5}$$

where ρ is charge density, $\mathbf{j}$ is current density and μ_0 is vacuum permeability.

Equations of motion for the particles are

$$\frac{\mathrm{d}\mathbf{x}_p}{\mathrm{d}t} = \mathbf{v}_p \tag{4.6}$$

$$\frac{\mathrm{d}\mathbf{p}_p}{\mathrm{d}t} = q_p(\mathbf{E} + \mathbf{v}_p \times \mathbf{B}), \tag{4.7}$$

where $\mathbf{v}_p$ is the velocity of p-th particle and $\mathbf{p}_p$ its momentum. The relativistic relation between velocity and momentum is

$$\mathbf{v_p} = \frac{1}{\gamma_p m_p} \mathbf{p}_p, \tag{4.8}$$

where γ is the Lorentz factor

$$\gamma_p = \sqrt{1 + \frac{\mathbf{p}_p^2}{(m_p c)^2}}.$$

For point particles, current and charge densities would be

$$\rho = \sum_p q_p \delta(\mathbf{x} - \mathbf{x}_p) \tag{4.9}$$

$$\mathbf{j} = \sum_p q_p \mathbf{v}_p \delta(\mathbf{x} - \mathbf{x}_p). \tag{4.10}$$

In generall, for every single particle indexed by p in the simulated system, the interaction with all of the other particles should be considered. For a typical 3D simulation of LWFA acceleration, where the simulation box size is 120 μm×80 μm×80 μm, and supposed plasma density is $n = 10^{19}$ cm^{-3}, totally $N \approx 10^{13}$ physical particles should be simulated. The system containing N particles would require approximately N^2 of their interactions. It would not be computationally feasible even for large HPC clusters.

Therefore the concept of macroparticles is introduced. Each macroparticle represent certain number of physical particles, typically 10^5 – 10^7 of them. It is a solid body with the certain momentum $\mathbf{p}_m$ spatially spread around its mean position $\mathbf{x}_m$. This spread is described as some normalized function $S(\mathbf{x})$ with bounded support .

When this reduction is applied, computational demands are lowered significantly. As an example let us consider that the grid resolution is 30 cells per wavelength of 0.8μm of Ti:sapphire laser in longitudinal direction and 3 cells per wavelength in transverse

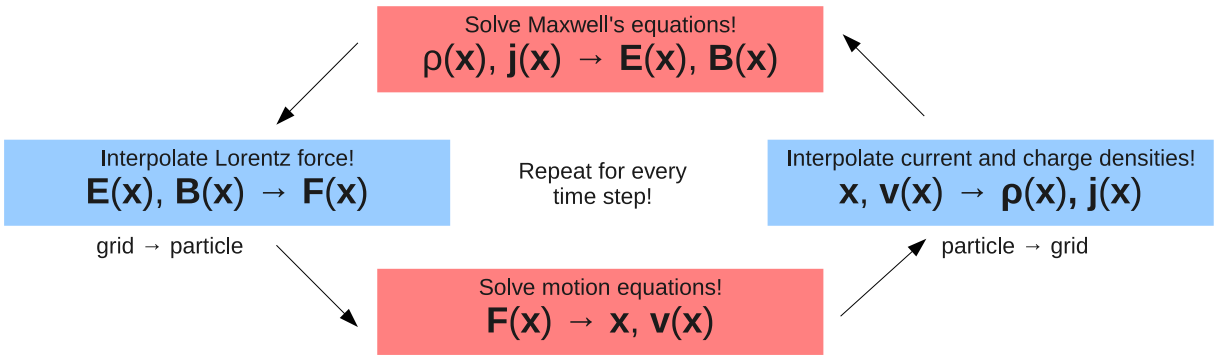

Figure 4.1: One cycle of the particle-in-cell method. Whereas charge and current densities and fields are interpolated at the grid, particle velocities and positions can be stored continuously in the simulation box.

directions. This grid contains 4.08×10^8 cells. Assuming 3 macroparticles per cell, there are 1.215×10^9 macroparticles to be simulated. This is feasible on the super-computers operating on ∼1,000 central processing units.

A further simplification and reduction of computational resources comes from the fact that the macroparticles do not interact directly with each other but only with the average electromagnetic field on the grid. The scaling thus changes from N^2 to const$\cdot N \cdot N_g$, where N_g is the number of grid points, which is usually much smaller than N. The constant depends in particular on the algorithm used to solve the Maxwell's equations and the order of the method.

In this thesis, most of the simulations were run in reduced 2D case. In a typical configuration, the simulation box of size 60 μm×36 μm was divided into 3,000×450 cells, with 3 macroparticles per cell. Such simulation requires approximately 750 CPUhours, and using 32 CPUs machine consumes 1 day of computational time. This simulations were performed using the services of National Grid Infrastructure MetaCentrum.

As a conclusion of this section, let us describe one cycle of the PIC method in plasma physics, it is schematically represented figure 4.1.

1. At the beginning, the positions $\mathbf{x_m}$ and the velocities $\mathbf{v_m}$ of individual macroparticles are known. The charge and current densities $\rho(\mathbf{x})$ and $\mathbf{j}(\mathbf{x})$ therefore can be calculated and interpolated on the grid.

2. Maxwell's equations are integrated on the grid to update the electric and magnetic fields $\mathbf{E}(\mathbf{x})$ and $\mathbf{B}(\mathbf{x})$. Whereas $\mathbf{E}$ is defined at integer timesteps $n\Delta t$, $\mathbf{B}$ is defined at half-integer timesteps $(n+1/2)\Delta t$. Additionally, charge and current densities are defined in specific points of space. Mostly those quantities are defined on the Yee lattice [Birdsall and Langdon, 2004]. Maxwell's equations are typically integrated using finite difference time domain (FDTD) method.

3. As the fields on the grid are known, the Lorentz force acting on individual macroparticles is calculated after the field is interpolated to their positions.

4. Lorentz force is the right hand side one of the motion equations. These equations are integrated mostly using the leap-frog scheme, Boris scheme [Boris, 1970] or Vay scheme [Vay, 2008]. Thus, the new values of the positions $\mathbf{x_m}$ and the velocities $\mathbf{v_m}$ of individual macroparticles are known.

4.2 Calculation of radiation properties

Method to calculate the angular and the frequency spectrum of the radiation $\frac{\mathrm{d}^2 I}{\mathrm{d}\omega \mathrm{d}\Omega}$ emitted by an electron bunch is based on the Fourier transform of the generated electric field. Mathematically it is expressed by the equation (3.18). This method is complementary to the alternative treatments proposed by Thomas [Thomas, 2010] and by Chen [Chen et al., 2013], which are based on the semi-analytical approach to the solution of the integral in (3.20). Proposed method can be however generalized to the construction of the spectrogram $\frac{\mathrm{d}^3 I}{\mathrm{d}t \mathrm{d}\omega \mathrm{d}\Omega}$ for special cases.

4.2.1 The principle of the method

The core of the method is to perform the Fourier transform of the quantity $\mathbf{E}(t)R(t)$. This quantity must be properly sampled in order to be able to calculate the spectrum of emitted X-rays. The minimum sampling frequency is determined by Whittaker–Nyquist-Kotelnikov–Shannon sampling theorem. A great overview of this mathematical theorem can be found e.g. in [Jerri, 1977]. It states that the accurate reconstruction of the continuous signal whose frequencies are limited is possible only if the sampling frequency is higher than twice the highest frequency component of the sampled signal. In practice, if the radiation energetic spectrum is to be calculated up to the energy 15 keV, the corresponding photon's frequency is 3.64×10^{18} Hz, sampling frequency of the signal should be 7.28×10^{18} Hz and it means that the length of the time step Δt of the electric field in the observer's spot has be at most 1.37×10^{-19} s. If the radiation bandwidth reaches as far as 1 MeV, such a time step has to be at most 2.06×10^{-21} s long.

Such a fine sampling is typically not obtained from the PIC simulations. Time step $\Delta t'$ is typically 10^{-16} s. Such a sampling frequency would be sufficient for the radiation up to 41 eV. Even if the transformation into the observer's time t is performed, the length of the time step is barely shorter than 10^{-18} s. Furthermore, sampling in the observer's time t is usually not equidistant anymore. The interpolation of the function $\mathbf{E}(t)R(t)$ must be carried out to obtain better sampling. Various interpolation methods may be used, however shape-preserving piecewise cubic interpolation seems to offer the satisfactory

results with the respect to the computational time needed. Once the signal $\mathbf{E}(t)R(t)$ is sampled properly, its fast Fourier transform can be computed.

A certain alternative for the low energy radiation can be non-uniform fast Fourier transform algorithm (NUFFT) [Fessler and Sutton, 2003]. However, this algorithm was not implemented.

4.2.2 Demonstration of the method

The results of this computations for various parameters of the electron trajectory are plotted in the figure 4.2. Zero-padding technique [Smith, 2007] was used to increase the resolution of spectra obtained via FFT. The electric field in the far field approximation was calculated using the radiation term in the formula (3.5). Without loss of generality, assume that the electron propagates in the x-direction and performs transverse betatron oscillations in the y-direction. Then $E_x/E_y \ll 1$ and $E_z/E_y \ll 1$,

$$|\mathfrak{F}[R(t)\mathbf{E}(t)](\omega)| \approx |\mathfrak{F}[R(t)E_y(t)](\omega)|\,.$$

Hence, the contribution of the electric field components E_x and E_y can be neglected. The quantity $E_y(t)R(t)$ is plotted in the left column. In the right column, corresponding spectrum on the axis of electron propagation is shown. The clear difference between undulator and wiggler regime is apparent. The electron trajectory was calculated using the model presented in [Corde et al., 2013] for the ambient electron density $n_e = 5{\times}10^{18}$ cm^{-3}. Electron propagated for 4 ps. The time duration t in the figure belongs to the observer. It is worth mentioning that this pulse duration decreases with the electron energy and grows with the oscillation amplitude.

In the case A, the electric field is continuous and the Fourier series comprise only of one harmonic. Electron has low energy $E_e = 10$ MeV and it oscillates with the amplitude 0.05 μm. The emitted radiation profile has sine-like shape with the peaks interconnected with the peaks of the electron's trajectory. The length of the observed signal is 4.8 fs. The only basic harmonic peak position is at 10.8 eV, it can be calculated from the theory as well [Esarey et al., 2002]. Electron performed eleven oscillations, the width of the line is $\Delta\omega/\omega = 1/11$. This case is known as an undulator regime, the K parameter is 0.066.

In the case B, electron energy is 25 MeV and its oscillation amplitude is 0.5 μm, the value of K is 1.0. The basic harmonic energy increases up to 26.1 eV and third, fifth seventh and ninth harmonics are present, since the even ones vanish. The third case C is close to the wiggler regime. Electron energy is 40 MeV, amplitude of oscillations is 1.2 μm, $K = 3.15$. It is still possible to distinguish single harmonics, however, their envelope has characteristic shape of the synchrotron radiation. The basic harmonic is 13.6 eV, the highest harmonic effectively present is approximately the 137th one with the energy 1.86 keV.

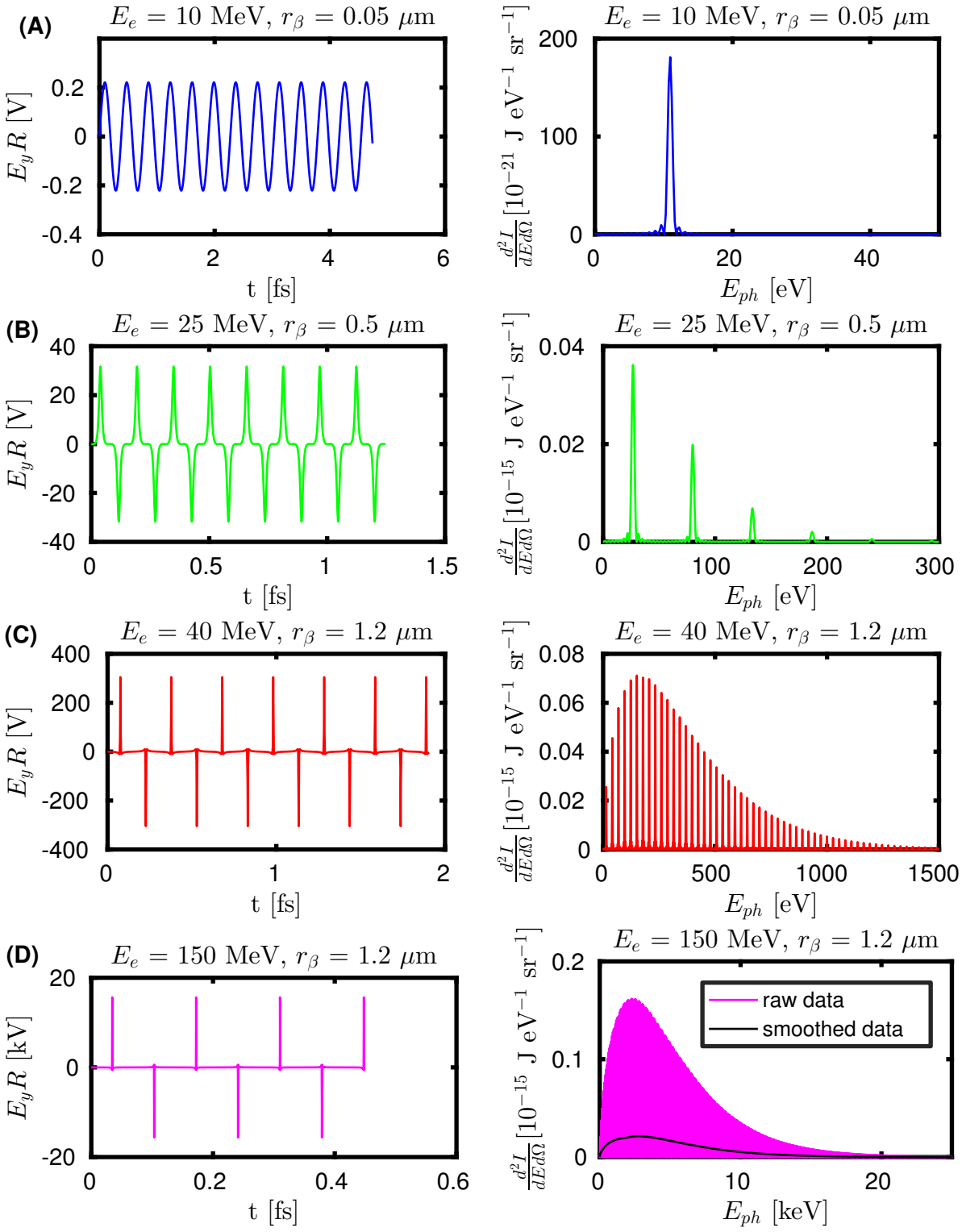

Figure 4.2: Electric field and radiated spectrum by a moving electron on axis for various electron energies and amplitudes of the betatron oscillations.

The case D represents example of wiggler regime with the $E_e = 150$ MeV, $r_\beta = 1.2$ μm and $K = 5.46$. The emitted radiation is comprised of many very closely spaced harmonics, therefore it can be considered as continuous synchrotron radiation. The black line in the figure represents smoothed spectrum. Critical energy of radiation is 2.70 keV, which is in the agreement with the expectation according to the formula (3.31). Furthermore, the high energy tail of the radiation reaches up to 20 keV, i.e. hard X-rays are generated. In this regime are the most contemporary experiment carried out, e.g. the experimental campaign at the PALS laser centre is aimed at this goal.

4.2.3 Simplification of the method for the wiggler case

The shape of the time dependence of the electric field is different for the undulator and wiggler regimes, it can be realised from the figure 4.2. In the wiggler case, the electron emits radiation almost exclusively in the turning points of its sine-like trajectory. Hence, there are only few very narrow time intervals which contribute significantly to the betatron radiation emission, while the rest can be neglected.

The radiated spectrum is calculated from the Fourier transform of the electric field according to the formula (3.18). Let us understand the signal of the radiation $u(t) = \mathbf{E}(t)R(t)$ as a sum of the contributions by single peaks $u_j(t)$.

$$u(t) = \sum_{j=1}^{N_p} u_j(t), \tag{4.11}$$

where N_p is number of peaks. Each contribution can be written as

$$u_j(t) = \begin{cases} \mathbf{E}(t)R(t) & |t - t_j| < \Delta t \\ 0 & \text{otherwise,} \end{cases} \tag{4.12}$$

where t_j is the time of the signal peak and Δt is a width of the considered peak. This width has to include whole peak and cannot overlap to its neighbours.

The equation for the radiated energy per solid angle (3.12) can be in this case reformulated to

$$\frac{\mathrm{d}\mathcal{E}}{\mathrm{d}\Omega} = c\varepsilon_0 \int_{-\infty}^{+\infty} \left| \sum_{j=1}^{N_p} u_j(t) \right|^2 \mathrm{d}t. \tag{4.13}$$

Thanks to the fact that the contributions of the single peaks do not overlap, the square of the absolute value of the sum of the contributions is equal to the sum of the squares of the single contributions

$$\frac{\mathrm{d}\mathcal{E}}{\mathrm{d}\Omega} = c\varepsilon_0 \int_{-\infty}^{+\infty} \sum_{j=1}^{N_p} |u_j(t)|^2 \,\mathrm{d}t \tag{4.14}$$

and thanks to the sum rule

$$\frac{\mathrm{d}\mathcal{E}}{\mathrm{d}\Omega} = c\varepsilon_0 \sum_{j=1}^{N_p} \int_{-\infty}^{+\infty} |u_j(t)|^2 \,\mathrm{d}t. \tag{4.15}$$

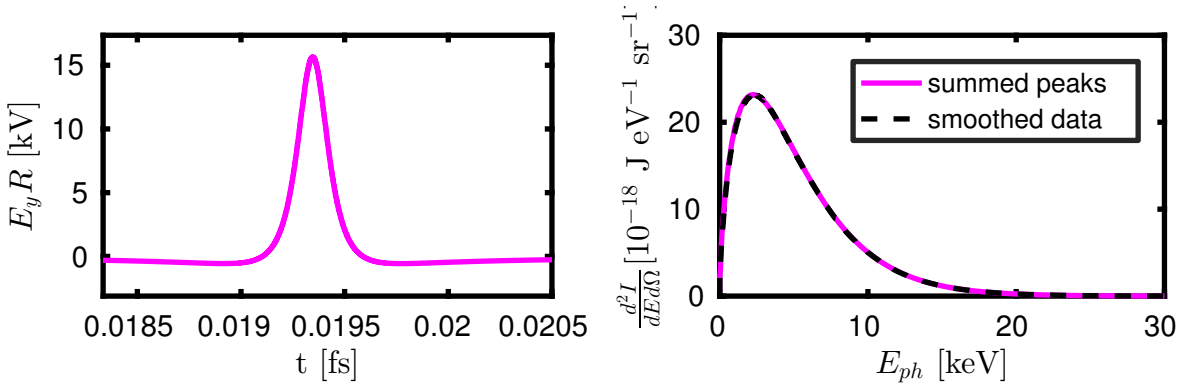

Figure 4.3: Left: One peak of the radiation signal $R(t)E_y(t)$ from the case D in the figure 4.2. Right: Its spectrum calculated as a sum of the contributions by single peaks (magenta solid) and a smoothed spectrum calculated according to the equation (3.18) using the Fourier transform of the whole signal (black dashed).

Using once again the Parseval's theorem (3.24) and sum rule in integration we obtain

$$\frac{\mathrm{d}\mathcal{E}}{\mathrm{d}\Omega} = \frac{c\varepsilon_0}{\pi} \sum_{j=1}^{N_p} \int_0^{+\infty} |\mathfrak{F}[u_j(t)](\omega)|^2 \,\mathrm{d}\omega = \int_0^{+\infty} \frac{c\varepsilon_0}{\pi} \left(\sum_{j=1}^{N_p} |\mathfrak{F}[u_j(t)](\omega)|^2 \right) \mathrm{d}\omega. \tag{4.16}$$

Hence the angular and frequency spectrum of the radiation is similar as in the relation (3.18)

$$\frac{\mathrm{d}^2 I}{\mathrm{d}\omega \mathrm{d}\Omega} = \frac{c\varepsilon_0}{\pi} \sum_{j=1}^{N_p} |\mathfrak{F}[u_j(t)](\omega)|^2 \,. \tag{4.17}$$

In conclusion, the calculation of the radiation emitted by single electron in the wiggler case can be simplified to the calculation of the sum of the contributions to the radiation emitted in N_p turning points of its sine-like trajectory

$$\frac{\mathrm{d}^2 I}{\mathrm{d}\omega \mathrm{d}\Omega} = \sum_{j=1}^{N_p} \left. \frac{\mathrm{d}^2 I}{\mathrm{d}\omega \mathrm{d}\Omega} \right|_j . \tag{4.18}$$

Therefore the most of the signal can be neglected, which is particularly helpful when high energy radiation is expected. The huge sampling rate places high demands on the memory. However, this simplification reduces the memory requirements rapidly.

The right hand of the figure 4.3 underlines this conclusion. The radiation spectrum of the 150 MeV electron oscillating with the betatron amplitude 1.2μm (case D from the figure 4.2) calculated as a sum of contributions to the radiation by single peaks is practically equal to its smoothed spectrum calculated according to the equation (3.18).

4.2.4 Spectrogram: temporal evolution of radiation profile

As we know from the equation (3.21), the radiation emitted by an electron bunch is equal to the sum of radiation emitted by all the individual electrons, if the incoherent nature

of the electron bunch is assumed. Adapting the simplification introduced in the Section 4.2.3, the total radiation emitted by electron bunch can be written as

$$\frac{\mathrm{d}^2 I}{\mathrm{d}\omega \mathrm{d}\Omega} = \sum_{i=1}^{N_e} \sum_{j=1}^{N_p} \left. \frac{\mathrm{d}^2 I}{\mathrm{d}\omega \mathrm{d}\Omega} \right|_{ij} = \sum_{k=1}^{N_e N_p} \left. \frac{\mathrm{d}^2 I}{\mathrm{d}\omega \mathrm{d}\Omega} \right|_{k}, \tag{4.19}$$

because it does not depend on the order of the summation. We can define the quantity radiated energy per unit frequency and per unit solid angle received during the time interval $t \in [\tau - \Delta t, \tau + \Delta t]$ as

$$\left. \frac{\mathrm{d}^2 I}{\mathrm{d}\omega \mathrm{d}\Omega} \right|_{t \in [\tau - \Delta t, \tau + \Delta t]} = \sum_{k | t_k \in [\tau - \Delta t, \tau + \Delta t]} \left. \frac{\mathrm{d}^2 I}{\mathrm{d}\omega \mathrm{d}\Omega} \right|_{k}. \tag{4.20}$$

Applying the limit transition $\Delta t \longrightarrow 0$, we can even define the quantity radiated energy per unit time per unit frequency and per unit solid angle as

$$\frac{\mathrm{d}^3 I}{\mathrm{d}t \mathrm{d}\omega \mathrm{d}\Omega} = \lim_{\Delta t \longrightarrow 0} \left. \frac{\mathrm{d}^2 I}{\mathrm{d}\omega \mathrm{d}\Omega} \right|_{t \in [\tau - \Delta t, \tau + \Delta t]}. \tag{4.21}$$

It means that the method to construct the spectrogram of the emitted radiation was designed. In practical implementation, every time moment t_k when the peak of the radiation by every single electron occurs is stored and total radiation received during time interval $t \in [t_{k_i}, t_{k_{i+1}}]$ is summed up applying the equation (4.20).

In general, all the radiation features can be calculated from the properties of the laser pulse and plasma combining PIC simulation with the particle tracking and this proposed post-processing analysis.

Chapter 5

Results

5.1 Experimental campaign at PALS

Experimental laser campaign was run at Ti:sapphire laser system located at PALS facility in Prague in 2016. The experimental setup was following: 50 fs, 0.6 J, 800 nm laser pulse interacted with the supersonic dry air. The measured electron density by Mach-Zehnder interferometry was in the focal spot rather high, varying around 5×10^{19} cm^{-3}. The laser beam was focused to the spot with the sizes (14.4±2.1) μm horizontally and (10.1±1.2) μm vertically. The energy delivered to the target in the region where $I > I_{max}/e^2$ was (366±30) mJ.

Highly stable electron bunches with the mean energy (17.4±1.1) MeV and energy spread (13.5±1.5) MeV was measured (see Fig. 5.1). Corresponding PIC simulations were carried out to support this observation. EPOCH 2D code with the field ionisation according to the ADK model [Ammosov et al., 1986] was employed.

The simulation started with a neutral gas (for simplicity, only nitrogen and oxygen atoms were used in their respective percentage) and the measured experimental parameters described above were used in the simulations. The simulated atoms were ionized by the 50 fs laser pulse containing the energy of 360 mJ in the focal spot with the waist of 7 μm and plasma with the electron density of 5.0×10^{19} cm^{-3} was created. The defined number of cells per wavelength was 30 in the longitudinal and 5 in transverse dimension with respect to the laser pulse propagation. Each cell contained one atom of oxygen and one atom of nitrogen, which after ionization typically results in 11 electrons per cell, considering ionisation energies of nitrogen and oxygen shown in Table 5.1.

Table 5.1: Ionisation energies of nitrogen and oxygen in electronvolts.

	1	2	3	4	5	6	7	8
N	14.53414	29.6013	47.44924	77.4735	97.8902	552.0718	667.046	
O	13.61806	35.11730	54.9355	77.41353	113.8990	138.1197	739.29	871.4101

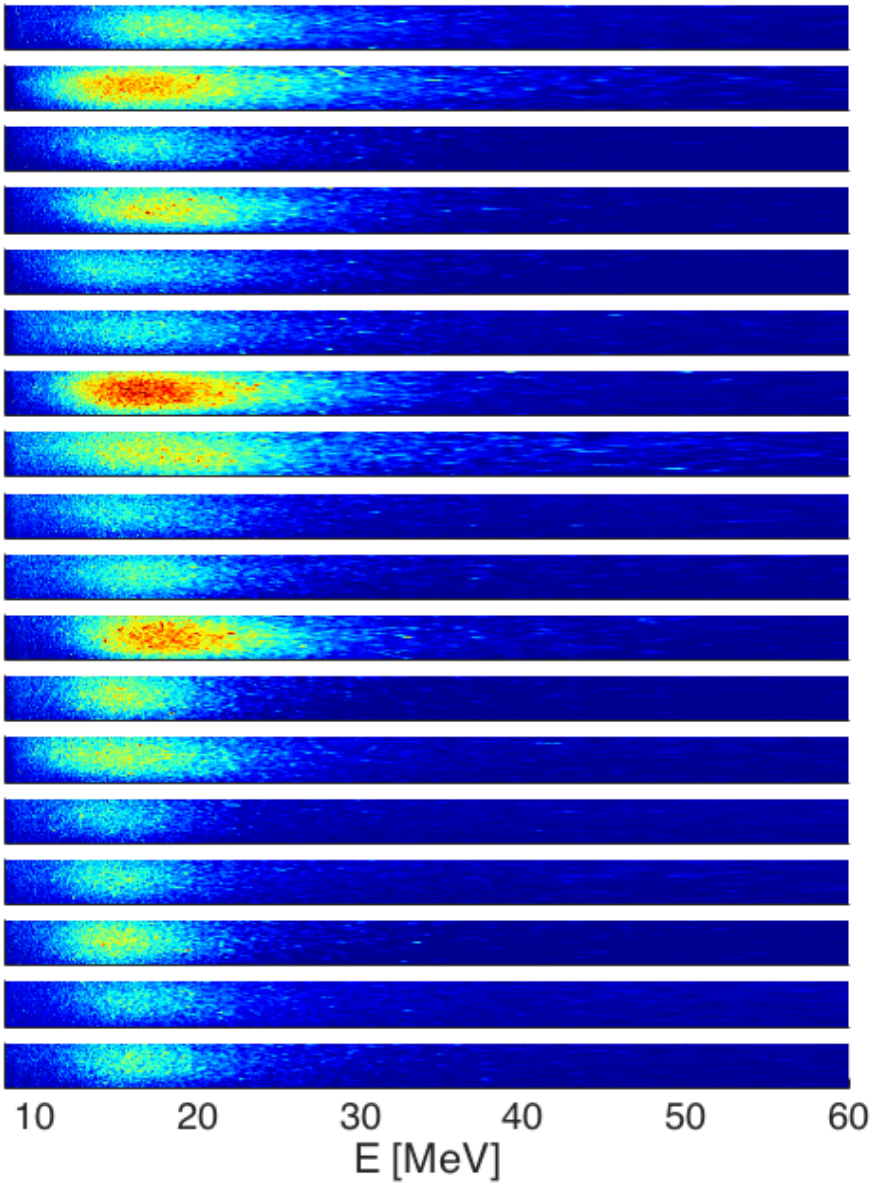

Figure 5.1: Typical electron spectra corrected on the beam pointing and obtained using the air gas jet target showing high energetic stability $\bar{E} = (17.4 \pm 1.1)$ MeV.

The peak electron energy of 17.1 MeV with the energy spread of 12.1 MeV obtained from the simulations were confronted with the measeured data (see Fig. 5.3). Good agreement is observed, however, neither the case is calibrated. The simulation indicates that formation of non-linear wake wave might occur (shown in Fig. 5.2), in which the trapped electrons could be accelerated. The peak energy sustained at the same value for all the time since the first electrons reached the center of the bubble. It happened very fast due to the low wake wave phase velocity determined by the high plasma density. The expected X-ray spectrum will be determined in the future. The results of this experiment and simulation will be published soon by K. Boháček et al.

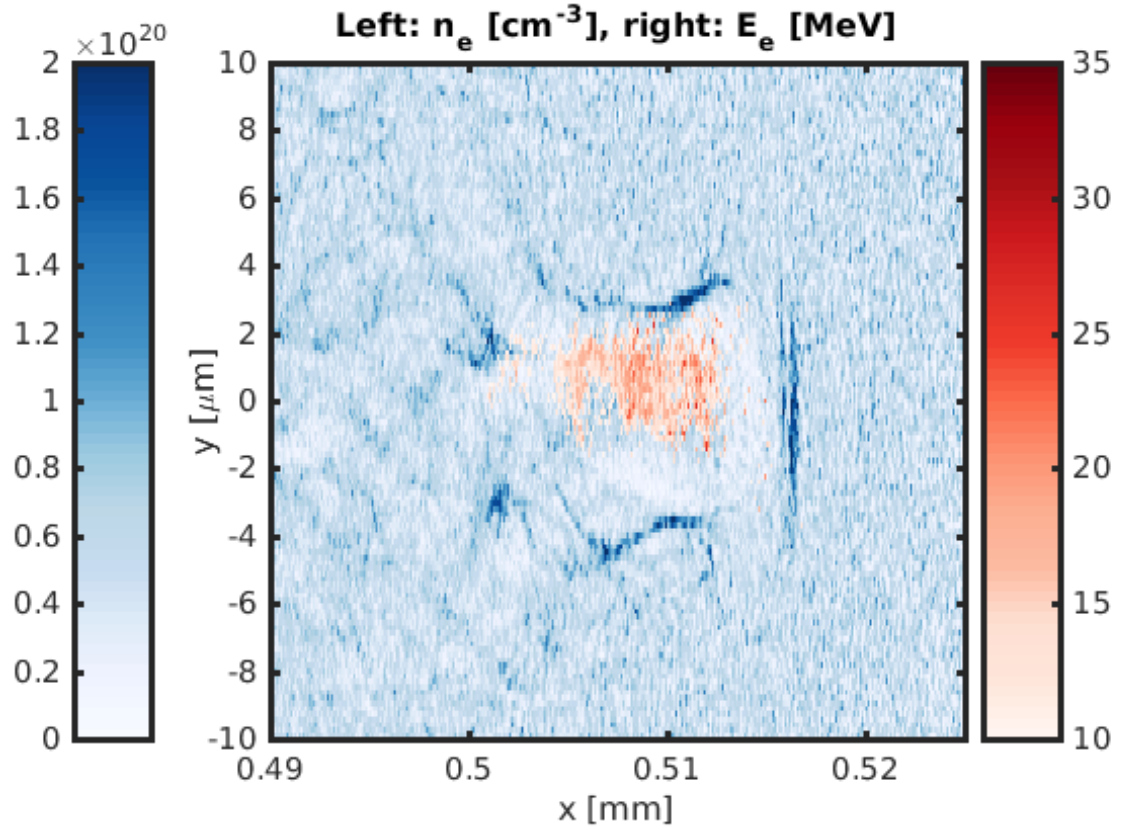

Figure 5.2: Electrons trapped due to an ionisation injection. (From simulation.)

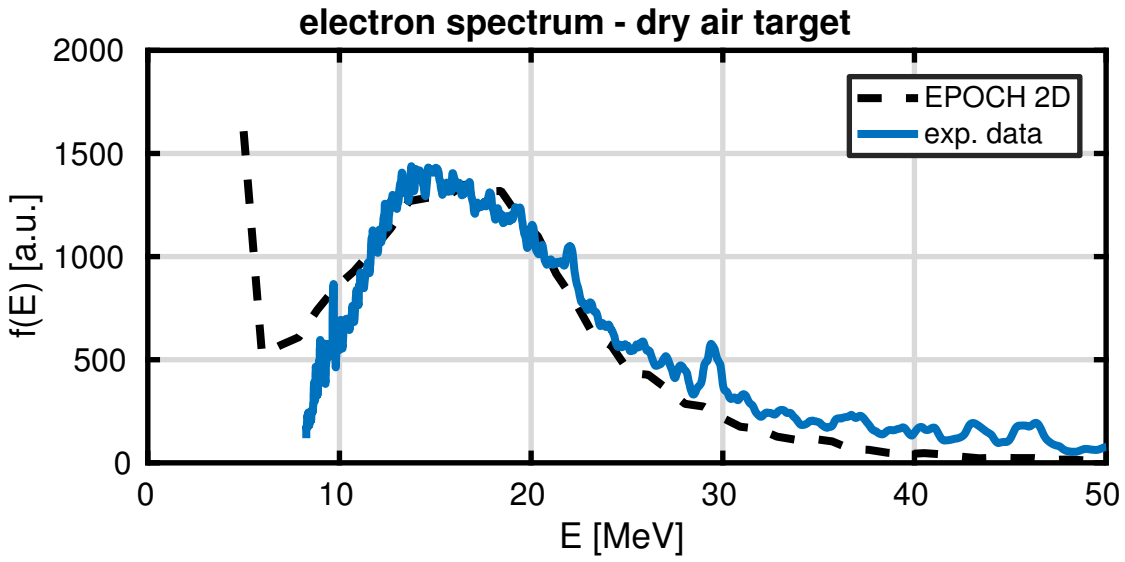

Figure 5.3: Electron spectra (blue solid) measured and simulated (black dashed).

5.2 Crossed beams

The optical injection model in crossed laser beams introduced in Section 2.4 was numerically studied and the influence on generated X-ray radiation was discussed and confronted with the other optical injection schemes using the numerical tools introduced in Section 4.

A typical case of the bubble regime achievable with standard ~ 100 TW laser systems was chosen for a demonstration of the injection mechanism: the plasma density $n_e = 5 \times 10^{18}$ cm^{-3}, the laser wavelength 0.8 μm, waist size $w_0 = 9.5$ μm, a pulse duration of 25 fs, and the MB intensity $a_0 = 4$ ($I = 3.42 \times 10^{19}$ W/cm^2).

The simulations were run using the EPOCH 2D PIC code with the subroutine implemented by author, which tracks the motion of selected trapped macroparticles. The computational time was provided by National Grid Infrastructure MetaCentrum. Post-processing and further computation of the emitted radiation features were run using the code developed by author implementing the theory introduced in the section 4.2.

5.2.1 Electron acceleration

Figure 5.4 shows the plasma density profile in the moving bubble at several simulation times for the case when no injection beam is present (left column, blue), and for the proposed configuration of the optical injection (right column, orange). The pump pulse came from the left, injection pulse from the bottom. Both laser beams focal spots are in [0,0]. The bunch injected by the injection beam is denoted by A. This bunch is trapped immediately after the time of interaction of both beams. Another bunch, denoted by B, appeared due to the self-injection at the simulation time about 5 ps in both cases.

Electrons in the second bunch and other bunches in the second and further bubbles at 6 ps gains much less energy than the optically injected bunch. Thus, the electron energy spectrum is divided into two parts and can be easily filtered. Furthermore, if the length of the plasma would be shorter than e.g. 1.3 μm (≈ 4.3 ps), no self-injection would occur at all and only very pure monoenergetic beam could be obtained.

Figure 5.5 shows the energy spectra of accelerated electrons. For crossing beams with the perpendicular polarization, the mean value of electron energy in the injected bunch A is about 400 MeV at 6 ps. The optimum ratio of intensities of pump and injection pulses I_{ALB}/I_{MB} was found at 0.01. With lower intensity of the injection pulse, the number of trapped electrons rapidly decreases. On the other hand, as the intensity of the injected pulse grows, the other characteristics of the produced electron beam like monochromacity and size worsen. Additionally, low intensity injection pulse does not disturb bubble dynamics and wakefield structure considerably.

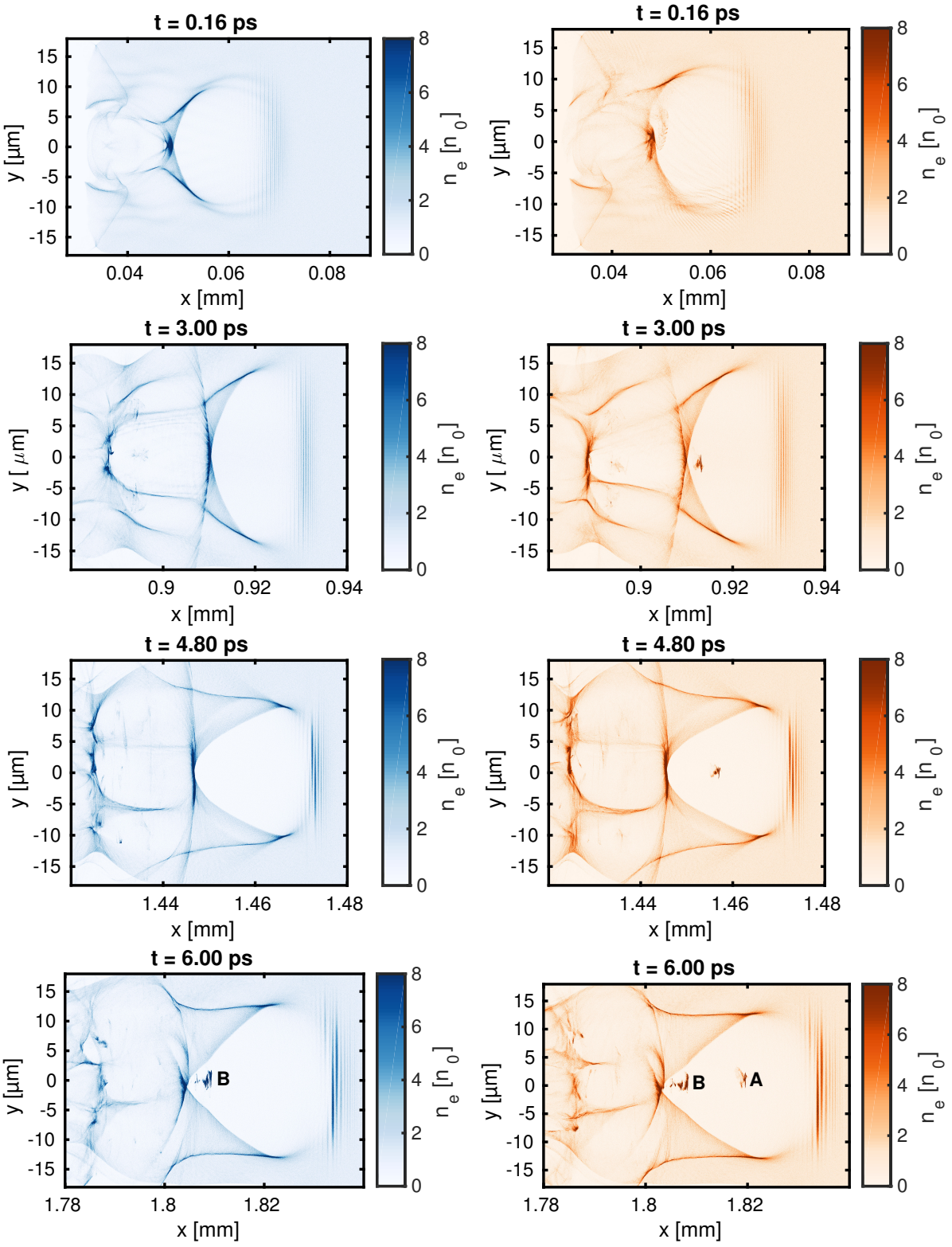

Figure 5.4: Evolution of the electron density for the case with the main beam only (blue) and the case when $I_{ALB} = 0.01 I_{MB}$ (orange). **A** - electron bunch injected by presented injection scheme. **B** - self-injected electron bunch. Injection pulse does not disturb bubble dynamics and self-injection when it is very weak in comparison with main beam.

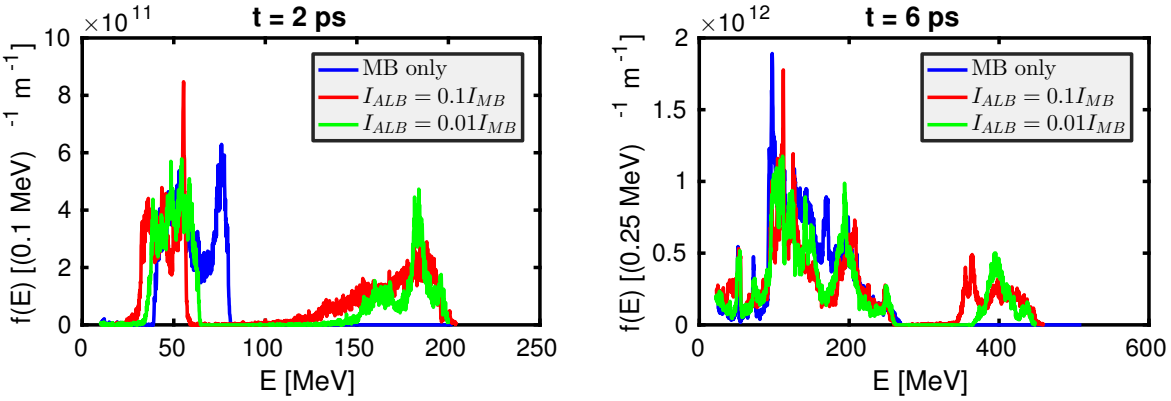

Figure 5.5: As the spectrum is divided into two parts, low energy part can be easily filtered and thus **narrow spectrum** obtained. I_{MB} is the intensity of the pump pulse, I_{ALB} is the intensity of injection pulse. Blue line represents the case when no injection pulse is present.
t =2 ps: $\overline{E_{el}} = 184$ MeV, $\sigma_{E_{el}} = 4$ MeV
t =6 ps: $\overline{E_{el}} = 394$ MeV, $\sigma_{E_{el}} = 10$ MeV.

5.2.2 Betatron radiation

Since the trapped electron bunches observed in the all the simulations mentioned above exhibit strong transverse oscillations in addition to their motion in the direction of the pump pulse propagation, they can be used for the generation of short X-ray pulses called betatron radiation. The physical mechanism was introduced in Section 3. The radiation spectrograms for three cases of the optical injection introduced in Section 2.4 are presented in Figure 5.6:

1. injection by transverse pulse with perpendicular polarization
2. injection by the transverse pulse with the parallel polarization
3. injection by a counter-propagating beam.

The time evolution of the radiation pulse and the energy spectra for the three cases are shown in Figure 5.7. The time interval of the radiation pulse is the shortest for the proposed configuration with perpendicular polarisations. Whereas the case of the parallel polarization exhibits longer X-ray pulse, the largest time interval is observed by the case of the counter-propagating beam injection.

In conclusion, the configuration of the optical injection by perpendicularly propagating and transverse polarised low intensity laser beam which does not significantly disturb a bubble dynamics was suggested. Compared to earlier proposed schemes, perpendicular propagation and parallel polarisation and counter-propagating 2-pulse scheme, the beams in this scheme possesses a higher bunch energy, the lower energy spread, and the injected charge is of the same order of magnitude.

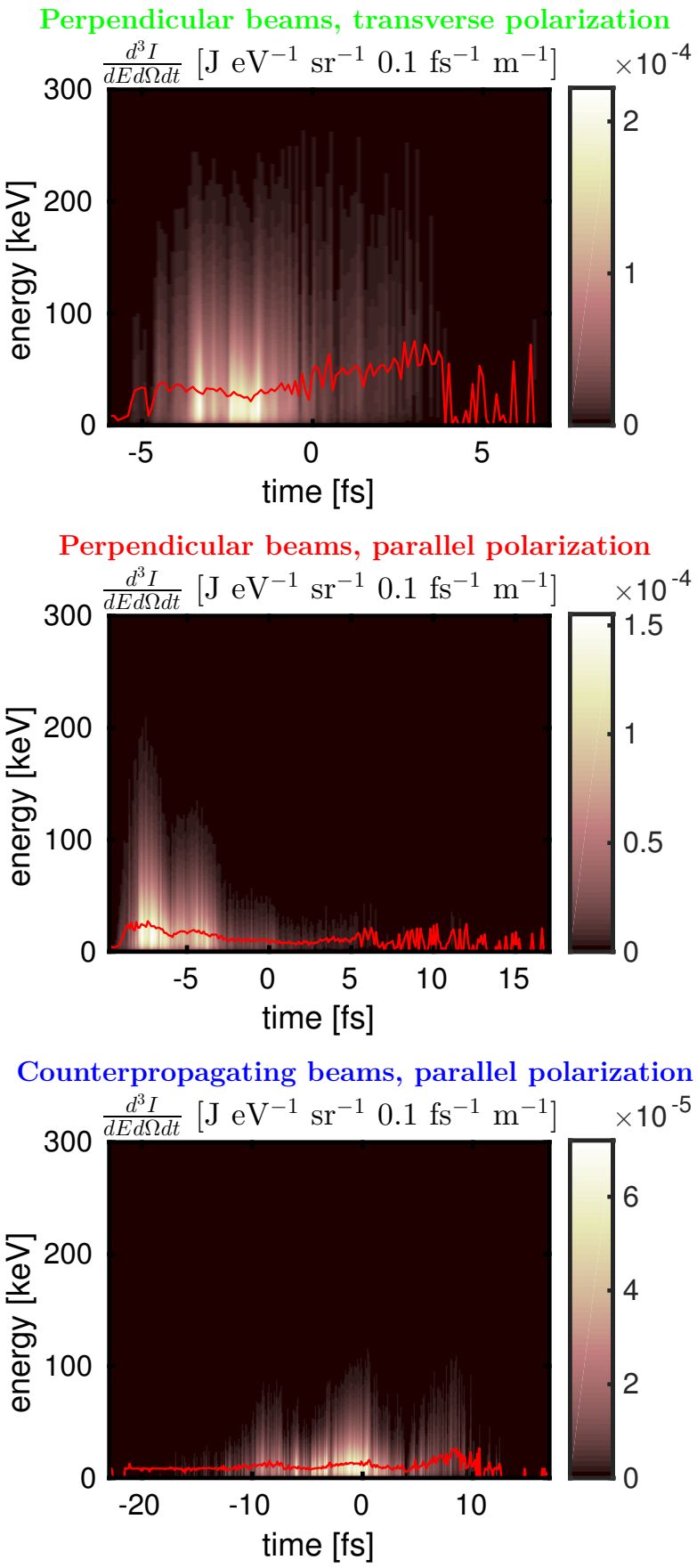

Figure 5.6: Betatron radiation spectrograms for compared configurations with the time evolution of critical energy (red solid).

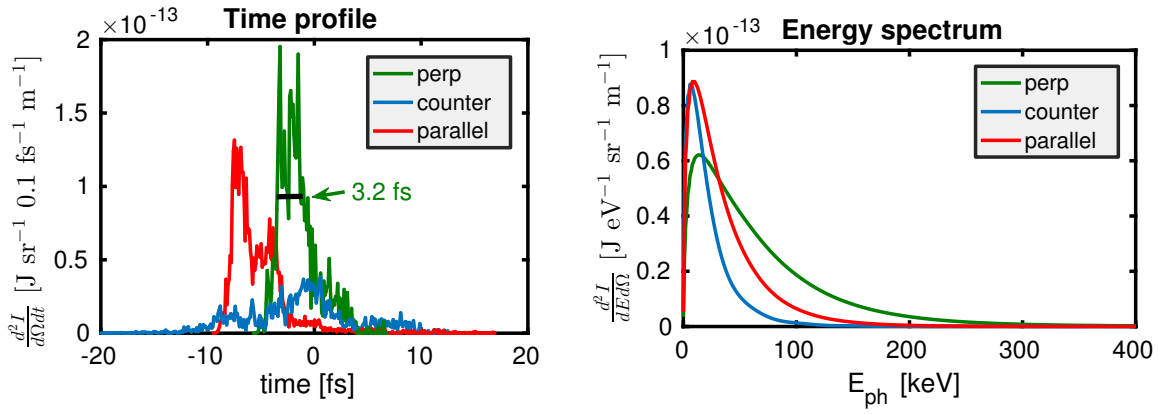

Figure 5.7: Left: Time profiles of X-ray pulses in configurations of the optical injection presented in Figure 5.6. Right: Energy spectra of the emitted X-rays for the same cases. Colours corresponds to the titles of individual spectrograms in Figure 5.6.

All numerical simulations indicate that with the consideration of the generated electron bunch properties, the X-ray bunch has appropriate features, i.e. it is shorter and it has higher critical energy.

Chapter 6

Conclusion

This study to doctoral thesis discusses the considered X-rays sources from the interaction of the intense laser pulses with plasma. Due to the the fact that most of the considered sources are based on the use of the accelerated electron bunches, a lot of attention is paid to the laser wakefield acceleration mechanism. Several injection schemes were reviewed, the most extensive search has been done in the branch of optical injection, where the method to improve the properties of generated electron bunch has been suggested. The injection pulse is intended to be directed orthogonally with respect to the main beam propagation direction and the polarisations of both pulses are proposed to be found in the plane of both beams propagation. The considerable improvement of the generated X-ray feature has been reported.

The theory of the radiation emitted by a moving charge was introduced. The method to construct the betatron radiation spectrograms in the wiggler limit based on the theory of retarded potentials was suggested, implemented and demonstrated. It enables to determine the features of the betatron radiation from the given laser pulse and plasma parameters in combination with the particle-in-cell simulation with the particle tracking. Furthermore, the code will be extended to enable the prediction of the properties of X-rays emitted due to the Thomson scattering as well. However, it is still needed to overcome several numerical issues rising from the high frequency of expected X-rays.

Although this work is rather theoretical, the connection with the experiment is maintained thanks to the author's participation on the grant project aimed on the generation of the tunable X-ray source from laser plasma. The simulations supporting the experimental results were and will be carried out. The experiment which demonstrated the acceleration of electrons in the dry air was performed already. Relevant simulation is in the good agreement with the measured data. Additionally, expected features of the generated X-rays will be computed soon.

As the features of the emitted X-rays are mainly determined by the properties of electron bunches, it is expected that the most of the work planned to the rest of author's

Ph.D. degree study will be dedicated to the improvement of the electron bunches quality by means of their emittance. Nevertheless, the codes calculating the properties of X-rays will be finished, tested, and used for the demonstration of generated X-ray beams properties.

Bibliography

[Ammosov et al., 1986] Ammosov, M., Delone, N. B., Krainov, V. P., et al. (1986). Tunnel ionization of complex atoms and of atomic ions in an alternating electromagnetic field. *Sov. Phys. JETP*, 64(6):1191–1194.

[Anania et al., 2014] Anania, M., Brunetti, E., Wiggins, S., Grant, D., Welsh, G., Issac, R., Cipiccia, S., Shanks, R., Manahan, G., Aniculaesei, C., et al. (2014). An ultrashort pulse ultra-violet radiation undulator source driven by a laser plasma wakefield accelerator. *Applied Physics Letters*, 104(26):264102.

[Arutyunian and Tumanian, 1963] Arutyunian, F. and Tumanian, V. (1963). The compton effect on relativistic electrons and the possibility of obtaining high energy beams. *Physics Letters*, 4(3):176–178.

[Attwood, 2007] Attwood, D. (2007). *Soft x-rays and extreme ultraviolet radiation: principles and applications*. Cambridge university press.

[Banerjee et al., 2012] Banerjee, S., Powers, N. D., Ramanathan, V., Ghebregziabher, I., Brown, K. J., Maharjan, C. M., Chen, S., Beck, A., Lefebvre, E., Kalmykov, S. Y., et al. (2012). Generation of tunable, 100–800 MeV quasi-monoenergetic electron beams from a laser-wakefield accelerator in the blowout regimea). *Physics of Plasmas (1994-present)*, 19(5):056703.

[Benedetti et al., 2013] Benedetti, C., Schroeder, C., Esarey, E., Rossi, F., and Leemans, W. (2013). Numerical investigation of electron self-injection in the nonlinear bubble regime. *Physics of Plasmas (1994-present)*, 20(10):103108.

[Birdsall and Langdon, 2004] Birdsall, C. K. and Langdon, A. B. (2004). *Plasma physics via computer simulation*. CRC Press.

[Boris, 1970] Boris, J. (1970). Relativistic plasma simulation-optimization of a hybrid code. In *Proc. Fourth Conf. Num. Sim. Plasmas, Naval Res. Lab, Wash. DC*, pages 3–67.

[Butler et al., 2002] Butler, A., Spence, D., and Hooker, S. (2002). Guiding of high-intensity laser pulses with a hydrogen-filled capillary discharge waveguide. *Physical Review Letters*, 89(18):185003.

[Chen et al., 2013] Chen, M., Esarey, E., Geddes, C. G. R., Schroeder, C. B., Plateau, G. R., Bulanov, S. S., Rykovanov, S., and Leemans, W. P. (2013). Modeling classical and quantum radiation from laser-plasma accelerators. *Physical Review Special Topics - Accelerators and Beams*, 16(3).

[Cipiccia et al., 2011] Cipiccia, S., Islam, M. R., Ersfeld, B., Shanks, R. P., Brunetti, E., Vieux, G., Yang, X., Issac, R. C., Wiggins, S. M., Welsh, G. H., et al. (2011). Gamma-rays from harmonically resonant betatron oscillations in a plasma wake. *Nature Physics*, 7(11):867–871.

[Corde et al., 2013] Corde, S., Phuoc, K. T., Lambert, G., Fitour, R., Malka, V., Rousse, A., Beck, A., and Lefebvre, E. (2013). Femtosecond x rays from laser-plasma accelerators. *Reviews of Modern Physics*, 85(1):1.

[D. et al., 2014] D., P., GhebregziabherI., GolovinG., LiuC., ChenS., BanerjeeS., ZhangJ., and P., U. (2014). Quasi-monoenergetic and tunable X-rays from a laser-driven Compton light source. *Nat Photon*, 8(1):28–31.

[Davoine et al., 2010] Davoine, X., Beck, A., Lifschitz, A., Malka, V., and Lefebvre, E. (2010). Cold injection for electron wakefield acceleration. *New Journal of Physics*, 12(9):095010.

[Esarey et al., 2009] Esarey, E., Schroeder, C., and Leemans, W. (2009). Physics of laser-driven plasma-based electron accelerators. *Reviews of Modern Physics*, 81(3):1229.

[Esarey et al., 2002] Esarey, E., Shadwick, B., Catravas, P., and Leemans, W. (2002). Synchrotron radiation from electron beams in plasma-focusing channels. *Physical Review E*, 65(5):056505.

[Faure et al., 2006] Faure, J., Rechatin, C., Norlin, A., Lifschitz, A., Glinec, Y., and Malka, V. (2006). Controlled injection and acceleration of electrons in plasma wakefields by colliding laser pulses. *Nature*, 444(7120):737–739.

[Fessler and Sutton, 2003] Fessler, J. A. and Sutton, B. P. (2003). Nonuniform fast fourier transforms using min-max interpolation. *Signal Processing, IEEE Transactions on*, 51(2):560–574.

[Fubiani et al., 2004] Fubiani, G., Esarey, E., Schroeder, C., and Leemans, W. (2004). Beat wave injection of electrons into plasma waves using two interfering laser pulses. *Physical Review E*, 70(1):016402.

[Harlow, 1964] Harlow, F. H. (1964). The particle-in-cell computing method for fluid dynamics. *Methods in computational physics*, 3(3):319–343.

[Hirose, 2011] Hirose, A. (2011). PHYS 812.3 - Electromagnetic Theory. `http://physics.usask.ca/~hirose/p812/p812fp.htm`. [Online; accessed 11-April-2016].

[Horný, 2014] Horný, V. (2014). Hot electron recirculation in the short intense pulse interactions with solid targets and its influence on k-α radiation. Master's thesis, Czech Technical University.

[Horný and Klimo, 2015] Horný, V. and Klimo, O. (2015). Hot electron refluxing in the short intense laser pulse interactions with solid targets and its influence on k-α radiation. *Nukleonika*, 60(2):233–237.

[Jackson, 1999] Jackson, J. D. (1999). *Classical electrodynamics*. Wiley.

[Jaroszynski et al., 2009] Jaroszynski, D. A., Bingham, R., and Cairns, R. (2009). *Laser-plasma interactions*. CRC Press.

[Jerri, 1977] Jerri, A. J. (1977). The shannon sampling theorem—its various extensions and applications: A tutorial review. *Proceedings of the IEEE*, 65(11):1565–1596.

[Ju, 2013] Ju, J. (2013). *Electron acceleration and betatron radiation driven by laser wakefield inside dielectric capillary tubes*. PhD thesis, Université Paris Sud-Paris XI.

[Kawamura et al., 2006] Kawamura, T., Horioka, K., and Koike, F. (2006). Potential of K-α radiation by energetic ionic particles for high energy density plasma diagnostics. *Laser and Particle Beams*, 24:261–267.

[Khan et al., 2006] Khan, S., Holldack, K., Kachel, T., Mitzner, R., and Quast, T. (2006). Femtosecond undulator radiation from sliced electron bunches. *Physical review letters*, 97(7):074801.

[Khrennikov et al., 2014] Khrennikov, K., Wenz, J., Buck, A., Xu, J., Heigoldt, M., Veisz, L., and Karsch, S. (2014). Tunable, all-optical quasi-monochromatic Thomson X-ray source. *arXiv preprint arXiv:1406.6654*.

[Kiselev et al., 2004] Kiselev, S., Pukhov, A., and Kostyukov, I. (2004). X-ray generation in strongly nonlinear plasma waves. *Phys. Rev. Lett.*, 93:135004.

[Kotaki et al., 2004] Kotaki, H., Masuda, S., Kando, M., Koga, J., and Nakajima, K. (2004). Head-on injection of a high quality electron beam by the interaction of two laser pulses. *Physics of Plasmas (1994-present)*, 11(6):3296–3302.

[Kuroda et al., 2011] Kuroda, R., Toyokawa, H., Yasumoto, M., Ikeura-Sekiguchi, H., Koike, M., Yamada, K., Yanagida, T., Nakajyo, T., Sakai, F., and Mori, K. (2011). Quasi-monochromatic hthisard X-ray source via laser Compton scattering and its application. *Nuclear Instruments and Methods in Physics Research Section A: Accelerators, Spectrometers, Detectors and Associated Equipment*, 637(1):S183–S186.

[Landau and Lifshitz, 1951] Landau, L. and Lifshitz, E. (1951). *The Classical Theory of Fields*. Addison-Wesley physics. Addison-Wesley Press.

[Lawson et al., 1979] Lawson, J. et al. (1979). Lasers and accelerators. *IEEE Trans. Nucl. Sci*, 26(3):4217–4219.

[Leemans et al., 2015] Leemans, W., Gonsalves, A., Nakamura, K., Mao, H.-S., Toth, C., Daniels, J., Mittelberger, D., Schroeder, C., Benedetti, C., Bulanov, S., et al. (2015). Multi-gev experiments with the petawatt class bella laser. In *2015 IEEE Photonics Conference (IPC)*, pages 59–60. IEEE.

[Lehe, 2014] Lehe, R. (2014). *Improvement of laser-wakefield accelerators: towards a compact free electron laser*. Theses, Ecole Polytechnique.

[Li et al., 2016] Li, X., Yu, Q., Gu, Y., Qu, J., Ma, Y., Kong, Q., and Kawata, S. (2016). Calculating the radiation characteristics of accelerated electrons in laser-plasma interactions. *Physics of Plasmas (1994-present)*, 23(3):033113.

[Lifschitz et al., 2009] Lifschitz, A. F., Davoine, X., Lefebvre, E., Faure, J., Rechatin, C., and Malka, V. (2009). Particle-in-Cell modelling of laser-plasma interaction using Fourier decomposition. *J. Comput. Physics*, 228(5):1803–1814.

[Lu et al., 2007] Lu, W., Tzoufras, M., Joshi, C., Tsung, F., Mori, W., Vieira, J., Fonseca, R., and Silva, L. (2007). Generating multi-gev electron bunches using single stage laser wakefield acceleration in a 3d nonlinear regime. *Physical Review Special Topics-Accelerators and Beams*, 10(6):061301.

[Macchi, 2013] Macchi, A. (2013). *A Superintense Laser-Plasma Interaction Theory Primer*. Springer Science & Business Media.

[Malka et al., 2008] Malka, V., Faure, J., Gauduel, Y. A., Lefebvre, E., Rousse, A., and Phuoc, K. T. (2008). Principles and applications of compact laser–plasma accelerators. *Nature Physics*, 4(6):447–453.

[Malka et al., 2005] Malka, V., Faure, J., Glinec, Y., Pukhov, A., and Rousseau, J.-P. (2005). Monoenergetic electron beam optimization in the bubble regimea). *Physics of Plasmas (1994-present)*, 12(5):056702.

[Malka et al., 2009] Malka, V., Faure, J., Rechatin, C., Ben-Ismail, A., Lim, J., Davoine, X., and Lefebvre, E. (2009). Laser-driven accelerators by colliding pulses injection: A review of simulation and experimental resultsa). *Physics of Plasmas (1994-present)*, 16(5):056703.

[Markidis and Lapenta, 2011] Markidis, S. and Lapenta, G. (2011). The energy conserving particle-in-cell method. *Journal of Computational Physics*, 230(18):7037–7052.

[Milburn, 1963] Milburn, R. H. (1963). Electron scattering by an intense polarized photon field. *Physical Review Letters*, 10(3):75.

[Mourou et al., 2006] Mourou, G. A., Tajima, T., and Bulanov, S. V. (2006). Optics in the relativistic regime. *Reviews of modern physics*, 78(2):309.

[Mulser and Bauer, 2010] Mulser, P. and Bauer, D. (2010). *High power laser-matter interaction*, volume 238. Springer Science & Business Media.

[Nakamura et al., 2007] Nakamura, K., Nagler, B., Tóth, C., Geddes, C., Schroeder, C., Esarey, E., Leemans, W., Gonsalves, A., and Hooker, S. (2007). Gev electron beams from a centimeter-scale channel guided laser wakefield acceleratora). *Physics of Plasmas (1994-present)*, 14(5):056708.

[Nikzad et al., 2012] Nikzad, L., Sadighi-Bonabi, R., Riazi, Z., Mohammadi, M., and Heydarian, F. (2012). Simulation of enhanced characteristic x rays from a 40-MeV electron beam laser accelerated in plasma. *Physical Review Special Topics-Accelerators and Beams*, 15(2):021301.

[Pak et al., 2010] Pak, A., Marsh, K., Martins, S., Lu, W., Mori, W., and Joshi, C. (2010). Injection and trapping of tunnel-ionized electrons into laser-produced wakes. *Physical review letters*, 104(2):025003.

[Paul et al., 2001] Paul, P. . M., Toma, E., Breger, P., Mullot, G., Augé, F., Balcou, P., Muller, H., and Agostini, P. (2001). Observation of a train of attosecond pulses from high harmonic generation. *Science*, 292(5522):1689–1692.

[Petržílka et al., 2002] Petržílka, V., Krlín, L., and Tataronis, J. (2002). Electron acceleration in a plane laser beam arising from randomizing the electron motion by an additional laser beam. In *Proc. Of the 29 th EPS Conference on Plasma Physics and Controlled Fusion (CD), paper P*, volume 1. Citeseer.

[Powers, 2014] Powers, N. D. (2014). Quasi-mono-energetic and Tunable Compton X-rays from a Laser Wakefield Accelerator. Copyright - Copyright ProQuest, UMI Dissertations Publishing 2014; Last updated - 2014-06-23; First page - n/a.

[Pukhov and Meyer-ter Vehn, 2002] Pukhov, A. and Meyer-ter Vehn, J. (2002). Laser wake field acceleration: the highly non-linear broken-wave regime. *Applied Physics B*, 74(4-5):355–361.

[Reich et al., 2007] Reich, C., Laperle, C. M., Li, X., Ahr, B., Benesch, F., and Rose-Petruck, C. G. (2007). Ultrafast x-ray pulses emitted from a liquid mercury laser target. *Optics letters*, 32(4):427–429.

[Rousse et al., 2004] Rousse, A., Phuoc, K. T., Shah, R., Pukhov, A., Lefebvre, E., Malka, V., Kiselev, S., Burgy, F., Rousseau, J.-P., Umstadter, D., et al. (2004). Production of a kev x-ray beam from synchrotron radiation in relativistic laser-plasma interaction. *Physical review letters*, 93(13):135005.

[Rousse et al., 2007] Rousse, A., Ta Phuoc, K., Shah, R., Fitour, R., and Albert, F. (2007). Scaling of betatron X-ray radiation. *The European Physical Journal D-Atomic, Molecular, Optical and Plasma Physics*, 45(2):391–398.

[Sarri et al., 2014] Sarri, G., Corvan, D., Schumaker, W., Cole, J., Di Piazza, A., Ahmed, H., Harvey, C., Keitel, C. H., Krushelnick, K., Mangles, S., et al. (2014). Ultrahigh brilliance multi-mev γ-ray beams from nonlinear relativistic thomson scattering. *Physical review letters*, 113(22):224801.

[Sävert et al., 2014] Sävert, A., Mangles, S., Schnell, M., Cole, J., Nicolai, M., Reuter, M., Schwab, M., Möller, M., Poder, K., Jäckel, O., et al. (2014). Direct imaging of the dynamics of a laser-plasma accelerator operating in the bubble-regime. *arXiv preprint arXiv:1402.3052*.

[Schick et al., 2016] Schick, D., Le Guyader, L., Pontius, N., Radu, I., Kachel, T., Mitzner, R., Zeschke, T., Schüßler-Langeheine, C., Föhlisch, A., and Holldack, K. (2016). Analysis of the halo background in femtosecond slicing experiments. *Journal of synchrotron radiation*, 23(3).

[Schoenlein et al., 2000] Schoenlein, R., Chattopadhyay, S., Chong, H., Glover, T., Heimann, P., Shank, C., Zholents, A., and Zolotorev, M. (2000). Generation of femtosecond pulses of synchrotron radiation. *Science*, 287(5461):2237–2240.

[Schultz and Vrakking, 2013] Schultz, T. and Vrakking, M. (2013). *Attosecond and XUV Spectroscopy: Ultrafast Dynamics and Spectroscopy*. John Wiley & Sons.

[Schumaker et al., 2014] Schumaker, W., Sarri, G., Vargas, M., Zhao, Z., Behm, K., Chvykov, V., Dromey, B., Hou, B., Maksimchuk, A., Nees, J., et al. (2014). Measurements of high-energy radiation generation from laser-wakefield accelerated electron beamsa). *Physics of Plasmas (1994-present)*, 21(5):056704.

[Shaw et al., 2016] Shaw, J., Lemos, N., Marsh, K., Tsung, F., Mori, W., and Joshi, C. (2016). Estimation of direct laser acceleration in laser wakefield accelerators using particle-in-cell simulations. *Plasma Physics and Controlled Fusion*, 58(3):034008.

[Smith, 2007] Smith, J. O. (2007). *Mathematics of the discrete Fourier transform (DFT): with audio applicaitons*. W3K Publishing.

[Spence and Hooker, 2000] Spence, D. and Hooker, S. (2000). Investigation of a hydrogen plasma waveguide. *Physical Review E*, 63(1):015401.

[Ta Phuoc et al., 2012] Ta Phuoc, K., Corde, S., Thaury, C., Malka, V., Tafzi, A., Goddet, J., Shah, R., Sebban, S., and Rousse, A. (2012). All-optical Compton gamma-ray source. *Nature photonics*, 6(5):308–311.

[Tajima and Dawson, 1979] Tajima, T. and Dawson, J. (1979). Laser electron accelerator. *Physical Review Letters*, 43(4):267.

[Thomas, 2010] Thomas, A. (2010). Algorithm for calculating spectral intensity due to charged particles in arbitrary motion. *Physical Review Special Topics-Accelerators and Beams*, 13(2):020702.

[Thomas et al., 2012a] Thomas, A., Ridgers, C., Bulanov, S., Griffin, B., and Mangles, S. (2012a). Numerical calculations of a high brilliance synchrotron source and on issues with characterizing strong radiation damping effects in non-linear thomson/compton backscattering experiments. *arXiv preprint arXiv:1204.5259*.

[Thomas et al., 2012b] Thomas, A., Ridgers, C., Bulanov, S., Griffin, B., and Mangles, S. (2012b). Strong Radiation-Damping Effects in a Gamma-Ray Source Generated by the Interaction of a High-Intensity Laser with a Wakefield-Accelerated Electron Beam. *Physical Review X*, 2(4):041004.

[Tsung et al., 2006] Tsung, F., Lu, W., Tzoufras, M., Mori, W., Joshi, C., Vieira, J., Silva, L., and Fonseca, R. (2006). Simulation of monoenergetic electron generation via laser wakefield accelerators for 5–25tw lasersa). *Physics of Plasmas (1994-present)*, 13(5):056708.

[Umstadter et al., 1996] Umstadter, D., Kim, J., and Dodd, E. (1996). Laser injection of ultrashort electron pulses into wakefield plasma waves. *Physical review letters*, 76(12):2073.

[Vauzour et al., 2014] Vauzour, B., Debayle, A., Vaisseau, X., Hulin, S., Schlenvoigt, H.-P., Batani, D., Baton, S., Honrubia, J., Nicolaï, P., Beg, F., et al. (2014). Unraveling resistive versus collisional contributions to relativistic electron beam stopping

power in cold-solid and in warm-dense plasmas. *Physics of Plasmas (1994-present)*, 21(3):033101.

[Vay, 2008] Vay, J.-L. (2008). Simulation of beams or plasmas crossing at relativistic velocitya). *Physics of Plasmas (1994-present)*, 15(5):056701.

[Wang et al., 2008] Wang, W.-M., Sheng, Z.-M., and Zhang, J. (2008). Controlled electron injection into laser wakefields with a perpendicular injection laser pulse. *Applied Physics Letters*, 93(20):201502.

[Wang et al., 2015] Wang, X., Du, D., Yi, S., Kalmykov, S., D'avignon, E., Fazel, N., Zagdzaj, R., Reed, S., Dong, P., Henderson, W., et al. (2015). Multi-gev electron generation using texas petawatt laser. *AIP 0Conference Proceedings*.

[Wang et al., 2013] Wang, X., Zgadzaj, R., Fazel, N., Li, Z., Yi, S., Zhang, X., Henderson, W., Chang, Y.-Y., Korzekwa, R., Tsai, H.-E., et al. (2013). Quasi-monoenergetic laser-plasma acceleration of electrons to 2 GeV. *Nature communications*, 4.

[Wang et al., 1997] Wang, Z., Zhang, Z., Xu, Z., and Lin, Q. (1997). Space-time profiles of an ultrashort pulsed gaussian beam. *Quantum Electronics, IEEE Journal of*, 33(4):566–573.

[Yu et al., 2014] Yu, T.-P., Hu, L.-X., Yin, Y., Shao, F.-Q., Zhuo, H.-B., Ma, Y.-Y., Yang, X.-H., Luo, W., and Pukhov, A. (2014). Bright tunable femtosecond x-ray emission from laser irradiated micro-droplets. *Applied Physics Letters*, 105(11):114101.

[Zhang et al., 2003] Zhang, P., Saleh, N., Chen, S., Sheng, Z., and Umstadter, D. (2003). An optical trap for relativistic plasma. *Physics of Plasmas (1994-present)*, 10(5):2093–2099.